Pharmacological Research 188 (2023) 106655

Contents lists available at ScienceDirect

Pharmacological Research

journal homepage: www.elsevier.com/locate/yphrs

Cannabidiol repairs behavioral and brain disturbances in a model of fetal alcohol spectrum disorder

Ani Gasparyan [a,b,c], Daniela Navarro [a,b,c], Francisco Navarrete [a,b,c], Amaya Austrich-Olivares [a], Ernest R. Scoma [d], Vedangi D. Hambardikar [d], Gabriela B. Acosta [e], María E. Solesio [d], Jorge Manzanares [a,b,c,*]

[a] Instituto de Neurociencias, Universidad Miguel Hernandez-CSIC, San Juan de Alicante, Alicante, Spain
[b] Redes de Investigación Cooperativa Orientadas a Resultados en Salud (RICORS), Red de Investigación en Atención Primaria de Adicciones (RIAPAd), Instituto de Salud Carlos III, MICINN and FEDER, Madrid, Spain
[c] Instituto de Investigación Sanitaria y Biomédica de Alicante (ISABIAL), Alicante, Spain
[d] Rutgers University, Department of Biology and CCIB, Camden, NJ, USA
[e] Instituto de Neurociencias Cognitiva y Traslacional (INCYT), CONICET, INECO, Universidad Favaloro, Ciudad Autónoma de Buenos Aires C1079ABE, Argentina

ARTICLE INFO

Keywords:
FASD
Cannabidiol
Animal model
Gene expression
Immunohistochemistry
Metabolomic analyses

ABSTRACT

Fetal alcohol spectrum disorder (FASD) includes neuropsychiatric disturbances related to gestational and lactational ethanol exposure. Available treatments are minimal and do not modulate ethanol-induced damage. Developing animal models simulating FASD is essential for understanding the underlying brain alterations and searching for efficient therapeutic approaches. The main goal of this study was to evaluate the effects of early and chronic cannabidiol (CBD) administration on offspring exposed to an animal model of FASD. Ethanol gavage (3 g/kg/12 h, p.o.) was administered to C57BL/6 J female mice, with a previous history of alcohol consumption, between gestational day 7 and postnatal day 21. On the weaning day, pups were separated by sex, and CBD administration began (30 mg/kg/day, i.p.). After 4–6 weeks of treatment, behavioral and neurobiological changes were analyzed. Mice exposed to the animal model of FASD showed higher anxiogenic and depressive-like behaviors and cognitive impairment that were evaluated through several experimental tests. These behaviors were accompanied by alterations in the gene, cellular and metabolomic targets. CBD administration normalized FASD model-induced emotional and cognitive disturbances, gene expression, and cellular changes with sex-dependent differences. CBD modulates the metabolomic changes detected in the hippocampus and prefrontal cortex. Interestingly, no changes were found in mitochondria or the oxidative status of the cells. These results suggest that the early and repeated administration of CBD modulated the long-lasting behavioral, gene and protein alterations induced by the FASD model, encouraging the possibility of performing clinical trials to evaluate the effects of CBD in children affected with FASD.

Abbreviations: 5HT1A, serotonergic receptor 1A; ASR, acoustic startle response; BDNF, brain-derived neurotrophic factor; CA_3, cornu ammonis 3; CA_1, cornu ammonis 1; CB1, cannabinoid receptor 1; CB2, cannabinoid receptor 2; CBD, cannabidiol; Cnr1, gene encoding cannabinoid receptor 1; Cnr2, gene encoding cannabinoid receptor 2; *Crf*, gene encoding for the corticotropin-releasing factor; DAB, 3,3′diaminobenzidine; DG, dental gyrus; ECS, endocannabinoid system; EtOH, ethanol; FAS, fetal alcohol syndrome; FASD, fetal alcohol spectrum disorder; GD, gestational day; HIPP, hippocampus; IPA, Ingenuity Pathway Analysis; i.p., intraperitoneal administration; KNN, k-nearest neighbors; LDB, light-dark box; LC-MS, liquid chromatography-mass spectrometry; MDA, malondialdehyde; Mfn2, mitofusin-2; mAb, monoclonal antibody; NAD, dependent deacetylase; NeuN, neurons neuronal nuclei; NF200, neurofilament 200; NOR, novel object recognition; NSFT, novelty suppressed feeding test; Nr3c1, gene encoding or the glucocorticoid receptor; OXPHOS, oxidative phosphorylation; PAE, perinatal alcohol exposure; PB, phosphate buffer; PFC, prefrontal cortex; PND, postnatal day; p.o., oral administration; PPAR, peroxisome proliferator-activated receptor; PVN, paraventricular nucleus; QC, quality control; RNA, ribonucleic acid; RT-PCR, real-time polymerase chain reaction; SDIA, step-down inhibitory avoidance; SEA-UMH, animal facilities service of the Universidad Miguel Hernández; Sirt3, sirtuin-3; SOD2, superoxide dismutase 2; THC, tetrahydrocannabinol; TOMM20, mitochondrial import receptor subunit TOM20; TRPV1, vanilloid receptor V1; TST, tail suspension test; VGluT1, vesicular glutamatergic transporter 1; VEH, vehicle; W, water.

* Correspondence to: Instituto de Neurociencias, Universidad Miguel Hernandez-CSIC, Avda. Ramón y Cajal s/n, San Juan de Alicante, 03550 Alicante, Spain.
E-mail address: jmanzanares@umh.es (J. Manzanares).

https://doi.org/10.1016/j.phrs.2023.106655
Received 9 December 2022; Received in revised form 31 December 2022; Accepted 10 January 2023
Available online 13 January 2023

1. Introduction

Perinatal alcohol exposure (PAE) is one of the most prevalent and avoidable risk factors for long-lasting somatic, behavioral and neurological abnormalities. Children exposed to PAE exhibit a wide range of symptoms, including impaired mental functions, emotional disturbances, and poorer memory, referred to as fetal alcohol spectrum disorders (FASD) [1–3]. The most severe form of FASD is fetal alcohol syndrome (FAS), which is associated with anatomical malformations, and cognitive and behavioral impairments [3]. The worldwide prevalence of FASD is estimated to be 7.7 per 1000 population, affecting approximately 5% of annual births [4]. This prevalence changes considerably depending on the study region, being considerably higher in the European Region and very low in the Eastern Mediterranean Region [5,6]. Moreover, the prevalence tends to increase over time. In a study conducted in the United States, the authors reported that 24–48 per 1000 first-grade students had FASD [7]. However, this prevalence increased a few years later to 31–98 per 1000 in the same study region [8]. These data reflect that FASD continues to be a major public health problem [9].

Currently, no treatments or established therapeutic tools exist to prevent and/or improve FASD-related outcomes. The pharmacotherapy of FASD tends to target specific behavioral problems, cognitive deficits, and emotional disturbances [10]. However, the long-lasting impact of these symptoms on children, adolescents, and their families is devastating [11]. Targeting the endocannabinoid system (ECS) by administering cannabinoid receptor agonists alleviates PAE-induced brain damage in animal models [12–16]. In addition, changes in ECS components (ligands and enzymes) are altered in different brain regions of offspring exposed to ethanol during their postnatal period [12–16]. All these results suggest that the ECS is strongly involved in the pathogenesis of FASD. Therefore, by manipulating this system, it could be possible to modulate some of the main features of this disorder.

Cannabidiol (CBD) is one of the main compounds of the *Cannabis sativa* plant, and it lacks addictive properties [17]. CBD presents a multimodal mechanism of action, interacting direct or indirectly with more than 65 different targets, such as cannabinoid receptors 1 (CB1) and 2 (CB2), serotonergic receptors 1A (5HT1A), vanilloid receptors TRPV1, and peroxisome proliferator-activated receptors (PPAR), among others [18]. This complex mechanism of action may contribute to its wide range of pharmacological effects, including but not limited to anxiolytic, antidepressant, antipsychotic, and neuroprotective effects [19]. Therefore, it is plausible to hypothesize that the administration of CBD may help treat some main PAE-induced features. Only one clinical study reported the potential usefulness of CBD in children and young adults with FASD. In this retrospective case series, the administration of CBD oil combined with tetrahydrocannabinol (THC) (in some patients) showed positive results in regulating the disruptive behavior associated with FASD [20]. In addition, in an animal model of PAE induced by the exposure of pregnant female mice to ethanol using drinking in the dark test, CBD was administered during early adolescence between postnatal days (PND) 25 and 34, modulating model-induced cognitive alterations [21]. However, there are no further studies evaluating CBD's utility in modulating or normalizing FASD-related emotional alterations nor identifying the molecular mechanisms underlying these actions.

In this study, we evaluated the effects of CBD in modulating the behavioral and neurobiological alterations in a new murine model of FASD, using a PAE paradigm by ethanol gavage administration (3 g/kg/12 h, p.o.) between the gestational day (GD) 7 and PND21 to pregnant females with a previous alcohol consumption history (voluntary ethanol consumption). We found significant emotional (anxiety, depression, and emotional hyperactivity) and cognitive (aversive and spontaneous recognition memories) alterations associated with changes in gene targets correlated with the stress-axis regulation and endocannabinoid system. In addition, a significant reduction in the number of cells, neurofilaments, neuroplasticity, and glutamatergic neurotransmission was found in the hippocampus (HIPP) of PAE-exposed male and female offspring. Changes in specific metabolic pathways in HIPP and prefrontal cortex (PFC) accompanied all these alterations.

The results reveal for the first time that CBD's early and chronic administration normalizes and partially repairs the neuronal damage induced by the FASD model observed at gene, cellular, metabolomic and behavioral levels. Thus, our findings strongly support the potential suitability of CBD in children and young adults with FASD and open opportunities for future clinical trials in this field.

2. Materials and methods

2.1. Animals

We used 190 C57BL/6 J male and female mice in all experiments. Fifty female and 20 male 5-week-old mice were purchased from Charles River laboratories (Lille, France). After their arrival, mice were individualized and left undisturbed for one week to acclimate to the animal housing room. Subsequently, females were exposed to a voluntary ethanol consumption paradigm before breeding began. A total of 120 offspring (60 males and 60 females) were obtained from the cross-breeding. All animals were maintained in the Animal Facilities Service of the Universidad Miguel Hernandez (SEA-UMH) under controlled environmental conditions of temperature (23 ± 2º C), humidity (60 ± 10%), and 12 h light-dark cycle (lights on from 08:00–20:00 h). All experimental procedures complied with the Spanish Royal Decree 53/2013, the Spanish Law 32/2007, and the European Union Directive of the 22nd of September 2010 (2010/63/UE) regulating the care of experimental animals and were approved by the Ethics Committee of Miguel Hernandez University. Animal studies are reported in compliance with the ARRIVE guidelines [22,23].

2.2. Perinatal alcohol exposure procedure

As previously described, female C57BL/6 J mice were exposed to voluntary ethanol consumption in a two-bottle choice paradigm from the PND 42 [24]. Female mice were individually housed in cages equipped with two feeding bottles containing only water to be acclimated and avoid possible stress. Afterward, animals were divided into two groups, one exposed to two bottles, both containing only tap water (n = 15), and another exposed to two bottles, one always containing tap water and the other containing increasing ethanol concentrations (2.5, 5, 7.5, and 10% of ethanol, 3 days each concentration) (n = 35). Bottles were alternated to prevent any place preference bias. Food was available ad libitum, and mice were weighed every 4 days. The volume of ethanol and water consumed was carefully measured and renewed daily. The ethanol consumed was calculated individually for each mouse, and the values were expressed as g/kg/day. The ratio of ethanol preference was also determined [ethanol preference: ethanol intake/ (ethanol intake + water intake)]. Once the 10% ethanol consumption and preference were stabilized for 15 days (or the equivalent period of water access in control animals), vaginal smears were collected in the afternoon for cytological evaluation for mouse estrous cycle staging identification, selecting only females with high ethanol consumption and preference. At this point, only 30 females from the initial 35 were selected. Those female mice at the pro-estrus or estrus stage of the cycle were placed into the cage of a singly housed male overnight, and the presence of a vaginal plug was monitored early in the morning. Pregnancy was determined by monitoring weight gain every 2 days and vaginal cytological evaluation. From GD7 until PND21, mothers previously exposed to voluntary ethanol consumption were administered 3 g/kg of ethanol (p.o., twice a day). In contrast, those not exposed to ethanol received tap water (p.o., twice a day) (Fig. 1). In the group of ethanol-exposed females, only 18 finished gestation and lactation periods properly, while in the control group, 11 of the initial 15 females did so.

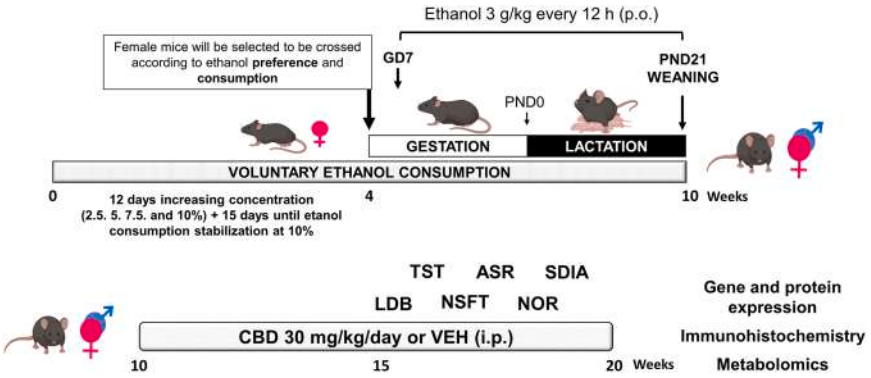

Fig. 1. Summary of the experimental design of the experimental procedures. Female mice were exposed to a voluntary ethanol consumption paradigm, achieving a stable 10% ethanol solution consumption and preference before crossing. After gestation confirmation, at GD7, ethanol gavage was started at a dose of 3 g/kg/12 h (p.o.) until the pup's weaning at PND21. Pups were treated with CBD 30 mg/kg/24 h (i.p.) or VEH from the day of weaning for 10 weeks. After the 5th week of treatment, behavioral evaluations were initiated to determine anxiety and depressive symptoms and cognitive alterations using different experimental paradigms and the effects of CBD on these behaviors. At the end of these behavioral studies, a group of mice was killed by cervical dislocation obtaining brain samples that were frozen for their use in the study of the gene, protein, and metabolomic analyses. Another group of mice was sacrificed by perfusion to obtain fixed brain samples and use them for the immunohistochemical studies. GD: gestational day, PND: post-natal day, p.o.: oral administration, i.p.: intraperitoneal administration, CBD: cannabidiol, LDB: light-dark box, TST: tail suspension test, NSFT: novelty suppressed feeding test, ASR: acoustic startle response, NOR: novel object recognition, SDIA: step-down inhibitory avoidance.

2.3. Blood ethanol concentrations (BEC)

On weaning day, female mice exposed to voluntary ethanol consumption and ethanol gavage during gestation and lactation received the last ethanol dose in the morning (3 g/kg, p.o.). One hour after ethanol administration, trunk blood was collected after rapid decapitation. Concentrations of ethanol were measured in plasma using an ethanol assay kit (Abcam, Cambridge, MA, USA) according to the manufacturer's instructions [17].

2.4. Cannabidiol (CBD) treatment of offspring

CBD was acquired from THC Pharm (Frankfurt, Germany) and dissolved in ethanol: cremophor: saline (1: 1: 18) to obtain the required 30 mg/kg dose. The drug was prepared daily immediately before its administration (between 17:00 and 19:00 h) at a volume of 10 ml/kg. After weaning, all the offspring obtained from the crossbreeding were separated by sex and housed in groups of 4–6 mice per cage. The daily treatment with CBD at 30 mg/kg or vehicle (VEH) (i.p.) was initiated on the same day. The behavioral evaluations started after 5 weeks of treatment with CBD that continued up to 10 weeks or until the end of the behavioral evaluation. Anxiety, depressive-like behaviors, and cognitive alterations were analyzed by the light-dark box (LDB), novelty suppressed feeding test (NSFT), tail suspension test (TST), acoustic startle response (ASR), novel object recognition (NOR), and step-down inhibitory avoidance (SDIA) tests that were realized in the morning (between 10:00 and 12:00 h). At the end of the behavioral evaluations, a group of mice was killed by cervical dislocation to obtain frozen brain samples and use them for gene expression (N = 7–9 animals/group) and protein quantification studies and metabolomics (N = 5–6 animals/group), respectively. Another group of animals was perfused to perform the immunohistochemical studies (N = 5–6 animals/group) (Fig. 1).

2.5. Emotional evaluation

2.5.1. Light-dark box (LDB)

This test assesses rodent anxiety-like behaviors by exposing them to an aversive environment [25–27]. LDB test was carried out using an apparatus with two methacrylate compartments (20 ×20×15 cm), one transparent and the other dark and opaque, separated by an opaque tunnel. The light compartment is illuminated with a lamp (60 W) placed 25 cm above it. Mice were placed in the lightbox facing the tunnel, and during 5-min sessions, the time spent in the lightbox and the number of transitions between both boxes were recorded.

2.5.2. Novelty-suppressed feeding test (NSFT)

This test measures anxiety-induced hyponeophagia as inhibiting food intake in an anxiety-provoking environment [26,28]. After 24 h of food deprivation, mice were placed in a transparent square cage (40 ×40×50 cm) with a single pellet in its center. The latency time before eating was recorded up to a threshold of 5 min. Once the mouse began eating, the amount of food pellet consumption was measured for another 5 min.

2.5.3. Tail suspension test (TST)

It is a widely accepted test to assess rodent depressive-like behaviors [27,29]. Mice were suspended by the tail individually at the edge of a lever above the tabletop (at 35 cm) using adhesive tape. The immobility time was measured for 6 min

2.5.4. Acoustic startle response (ASR)

A previously described protocol was used [26,30]. Briefly, mice were placed in soundproof chambers equipped with loudspeakers controlled by STARTLE software (Panlab, Barcelona, Spain). Mice were placed into Plexiglas cylinders, and their movements were measured by a piezoelectric accelerometer and converted into a digital signal. After a 3-day acclimatization period (5 min into the cage), mice were exposed to 10 trials of 120 dB (40 ms, 8000 Hz) of acoustic startle stimulus every 44 s. The maximum startle amplitude during a 100 ms sampling window was recorded.

2.6. Cognitive evaluation

2.6.1. Novel object recognition (NOR)

It is an accepted and frequently used test to assess recognition memory [31]. During the habituation phase, mice were exposed to a square cage with two identical objects (named familiar objects), recording the exploration time of each object for 5 min. Similarly, the exploration time of both objects was measured for 5 min, calculating the discrimination index as Discrimination Index= (New object exploration time – Familiar Object exploration time)/ (New object exploration time + Familiar Object exploration time). After 24 h, mice were re-exposed to the same cage changing one of the familiar objects for a new one.

2.6.2. Step-down inhibitory avoidance (SDIA)

This test was described by Izquierdo and colleagues [32]. It consisted of an acrylic box (50 ×25×25 cm) with a floor composed of a grid of parallel stainless-steel bars, 1 mm in diameter and 1 cm apart. In the habituation phase, animals were placed on the platform and immediately upon stepping down, they received a foot shock (0.5 mA for 2 s). Mice were returned to the home cage after 24 h to evaluate the

long-term aversive memory.

2.7. Gene expression analyses by RT-PCR

Relative gene expression of corticotropin-releasing factor (*Crf*) in the paraventricular nucleus (PVN), glucocorticoid receptor (*Nr3c1*), cannabinoid receptors 1 (*Cnr1*) and 2 (*Cnr2*) and peroxisome proliferator-activated receptor delta (*Ppard*) in the hippocampus (HIPP) were analyzed by real-time polymerase chain reaction (RT-PCR). At the end of the experimental procedures and 14–16 h after the last drug administration (CBD or VEH), a group of mice was killed by cervical dislocation. Brains were removed from the skull and frozen at − 80ºC. These samples were cut in a cryostat (−10ºC), obtaining coronal sections of 500 μm following the atlas of Paxinos and Fraklin [26,33] and were microdissected following the procedure described by Palkovits and previously performed by our group [34,35]. Total ribonucleic acid (RNA) was extracted with TRI Reagent extraction, and reverse transcription was carried out (Applied Biosystems, Madrid, Spain). Quantitative analyses of the relative gene expression of *Crf* (Mm01293920_s1), *Nr3c1* (Mm00433832_m1), *Cnr1* (Mm00432621_s1), *Cnr2* (Mm00438286_m1) and *Pparβ/δ* (Mm00803184_m1) genes was performed on the StepOne Sequence Detector System (Applied Biosystems, Madrid, Spain). Data for each target gene was normalized to the endogenous reference gene 18 S (Mm03928990_g1), and the fold change in target gene expression was determined using the 2-ΔΔCt method [36].

2.8. Conventional and confocal immunohistochemistry

This study focused on HIPP's dentate gyrus (DG), cornu ammonis 3 (CA_3), and CA_1 regions. The general criteria reported by Amaral and Wittler were used to define the hippocampal areas and strata [37].

Briefly, 12–14 h after the last administration of the corresponding drug (CBD or VEH), adult male and female mice were weighed, anesthetized with isoflurane, and intracardially perfused with 50 ml of saline followed by 250 ml of 4% paraformaldehyde, 0.1 M sucrose, and 0.002% $CaCl_2$ in 0.1 M phosphate buffer (PB; 1.4% K_2HPO_4 14 g/L, $NaH_2PO_4$0.2 H_2O ~3 g/L to pH 7.3–7.4). Brains were dissected, post-fixed by immersion in the same perfusion medium at room temperature for 4 hr and then stored in 0.05% sodium azide in PB at 4 °C. Eight parallel series of coronal sections containing the rostromedial portion of the DG and CA (−1.8 to-2.30 from Bregma) were cut with a Microm HM 650 V vibratome (Thermo Fisher Scientific, Inc., Barcelona, Spain) at 50 μm and stored in 0.05% sodium azide in PB at 4 °C. One series was immunostained with anti-mature neurons neuronal nuclei (NeuN) monoclonal antibody (mAb) (1:400; Chemicon International Inc., Temecula, CA). Immunolabeled sections were incubated with biotinylated horse anti-mouse Ab (1:150), Vectastain ABC kit (1:200; both from Vector Laboratories, Inc., Burlingame CA), and 0.05% 3,3′diaminobenzidine (DAB, Sigma-Aldrich Co.). The sections were mounted on gelatinized slides, air dried for 24 h, dehydrated in ethanol, cleared in xylol, and coverslipped. The adjacent series were immunostained for fluorescence, starting with guinea pig anti-vesicular glutamatergic transporter one antibody (VGluT1; 1:5000; Millipore, Temecula, CA). All sections were incubated with goat anti-guinea pig antibody, Alexa Fluor 488 (1:200, Molecular Probes, Invitrogen, Barcelona, Spain). Rabbit anti-neurofilament 200 antibody (NF200; 1:500; Sigma-Aldrich) was used to label neurofilament, and rabbit anti-BDNF (1:400, Millipore Corp, USA) antibody for brain-derived neurotrophic factor. All sections were then incubated with goat anti-rabbit antibody, Alexa Fluor 488 (1:200, Molecular Probes, Invitrogen, Barcelona, Spain).

Sections were mounted using ProLong Gold (Molecular Probes, Invitrogen). All samples were examined in a Leica SPEII confocal laser fluorescence microscope, with images captured using Leica Application Suite X software.

2.9. Immunoblots

Brains were homogenized, and immunoblot assays were performed following the same protocol previously used [38–40]. In this case, the following primary antibodies were used: superoxide dismutase 2 (SOD2) (Sigma Millipore, St. Louis, MI, USA. Cat. number: 06–984), oxidative phosphorylation (OXPHOS) cocktail (Abcam, Cambridge, UK. Cat. number: ab110413), mitochondrial import receptor subunit TOM20 (TOMM20) (Cell Signaling Technology, Danvers, MA, USA. Cat. number: 42406), Sirt3 (sirtuin-3) (Cell Signaling Technology, Danvers, MA, USA. Cat. number: 5490), and mitofusin-2 (Mfn2) (Abcam, Cambridge, UK. Cat. number: ab56889). As a loading control, we used β-Actin (Cell Signaling Technology, Danvers, MA, USA. Cat. number: 3700). Anti-mouse and Anti-rabbit secondary antibodies were purchased from BioRad (Hercules, CA, USA). Cat. numbers for these antibodies are 1706516 and 1706515, respectively. Signal quantification was performed using ImageJ (NIH, Bethesda, MA, USA) and following a previously described protocol [41]. Individual outliers (+/- 2 x STED) were not considered for the statistical analysis (Supplementary Information).

2.10. Lipid peroxidation assay

Lipid peroxidation was assayed by measuring the presence of malondialdehyde (MDA), a well-known final subproduct of this metabolic pathway. Samples were prepared similarly to a previous protocol [40]. Subsequently, the concentrations of MDA were measured using the lipid peroxidation assay kit (Abcam, Cambridge, UK. Cat. number: ab118970) and following the manufacturer's specifications. The results were visualized using a BioTek spectrophotometer (Thermo Fisher Scientific, Waltham, MA, USA) (Supplementary Information).

2.11. Targeted metabolomics

Biological triplicates were used to conduct these experiments. Samples were frozen, homogenized, and shipped overnight on dry ice for metabolomics assay to the Northwest Metabolomics Research Center (University of Washington, Seattle, WA, USA). At that facility, a metabolomics assay was performed, as previously reported, using appropriate internal controls [39,42]. Briefly, aqueous metabolites for targeted liquid chromatography-mass spectrometry (LC-MS) analysis were extracted using a protein precipitation method similar to the one described elsewhere [43,44]. Samples were first homogenized in 200 μL purified deionized water at 4 °C, then 800 μL of methanol containing 6 C_{13}-glucose and 2 C_{13}-glutamate (internal reference standards) was added. Afterward, samples were vortexed, stored for 30 min at − 20 °C, sonicated in an ice bath for 10 min, centrifuged for 15 min at 14, 000 rpm and 4 °C, and then 600 μL of supernatant was collected from each sample. Lastly, recovered supernatants were dried on a SpeedVac and reconstituted in 1.0 ml of LC-matching solvent containing 2 C_{13}-tyrosine and 3 C_{13}-lactate (reference internal standards). Protein pellets left over from the sample prep were saved for BCA protein assay. Subsequently, targeted LC-MS metabolite analysis was performed on a duplex-LC-MS system composed of two Shimadzu UPLC pumps, CTC Analytics PAL HTC-xt temperature-controlled auto-sampler and AB Sciex 6500 + Triple Quadrupole MS equipped with ESI ionization source [44]. UPLC pumps were connected to the auto-sampler in parallel to perform two chromatography separations independently. Each sample was injected twice on two identical analytical columns (Waters XBridge BEH Amide XP), performing separations in hydrophilic interaction liquid chromatography (HILIC) mode. While one column completed separation and MS data acquisition in ESI+ ionization mode, the other column was equilibrated for sample injection, chromatography separation and MS data acquisition in ESI- mode. Each chromatography separation was 18 min (total analysis time per sample was 36 min). MS data acquisition was performed in multiple-reaction monitoring (MRM) mode. LC-MS system was controlled using AB

Sciex Analyst 1.6.3 software. Measured MS peaks were integrated using AB Sciex MultiQuant 3.0.3 software. The LC-MS assay targeted 361 metabolites (plus 4 spiked reference internal standards). The study samples measured up to 178 metabolites and 4 reference standards. In addition to the study samples, two sets of quality control (QC) samples were used to monitor the assay performance and data reproducibility. One QC [QC(I)] was a pooled human serum sample used to monitor system performance, and the other QC [QC(S)] was pooled study samples. This QC was used to monitor data reproducibility. Each QC sample was injected per every 10 study samples. Data were well reproducible, with a median CV of 5.3%. Generated MS data were normalized vs. BCA total protein count.

Data were subsequently analyzed at the Rutgers laboratory, and figures were created using Metabolome (MetaboAnalyst, University of Alberta, Canada) and Ingenuity Pathway Analysis (IPA, Qiagen, Hilden Germany). In the case of MetaboAnalyst, features with > 30% missing values were removed. Those within the range were estimated using k-nearest neighbors (KNN). After this, no further outliers were manually removed. Data were normalized by protein count, and fold change was set up at 2.0 and *p*-value at 0.05. To create the predictions using IPA, the *p*-value was set up at 0.5, which allowed us to use between 200 and 300 metabolites from each experimental group to conduct the analysis.

2.12. Statistical analyses

Statistical analyses were performed using SigmaPlot 11.0 version for all the data except metabolomics (see the corresponding section). The Student's t-test was used to compare two groups, one-way variance analyses (ANOVA) to compare 3 or more groups, followed by Student-Newman-Keul's test for the posthoc analyses. Differences were considered significant if the type 1 error or alpha probability was less than 5%.

3. Results

3.1. Behavioral evaluations

3.1.1. Emotional evaluation

3.1.1.1. Light-dark box (LDB). Perinatal ethanol exposure reduced the time in the lighted box in both males (Fig. 2A, one-way ANOVA, $F(2,44) = 7.359$, $P = 0.002$) and females (Fig. 2B, one-way ANOVA, $F(2,44) = 13.140$, $P < 0.001$) adult mice, without changing the number of transitions between both boxes (males Fig. 2C, one-way ANOVA, $F(2,44) = 1.715$, $P = 0.192$; females Fig. 2D, one-way ANOVA, $F(2,44) = 0.000$, $P = 1.000$). In both cases, CBD chronic administration increased the time in the lighted box, reaching values similar to those obtained in control or W-VEH animals.

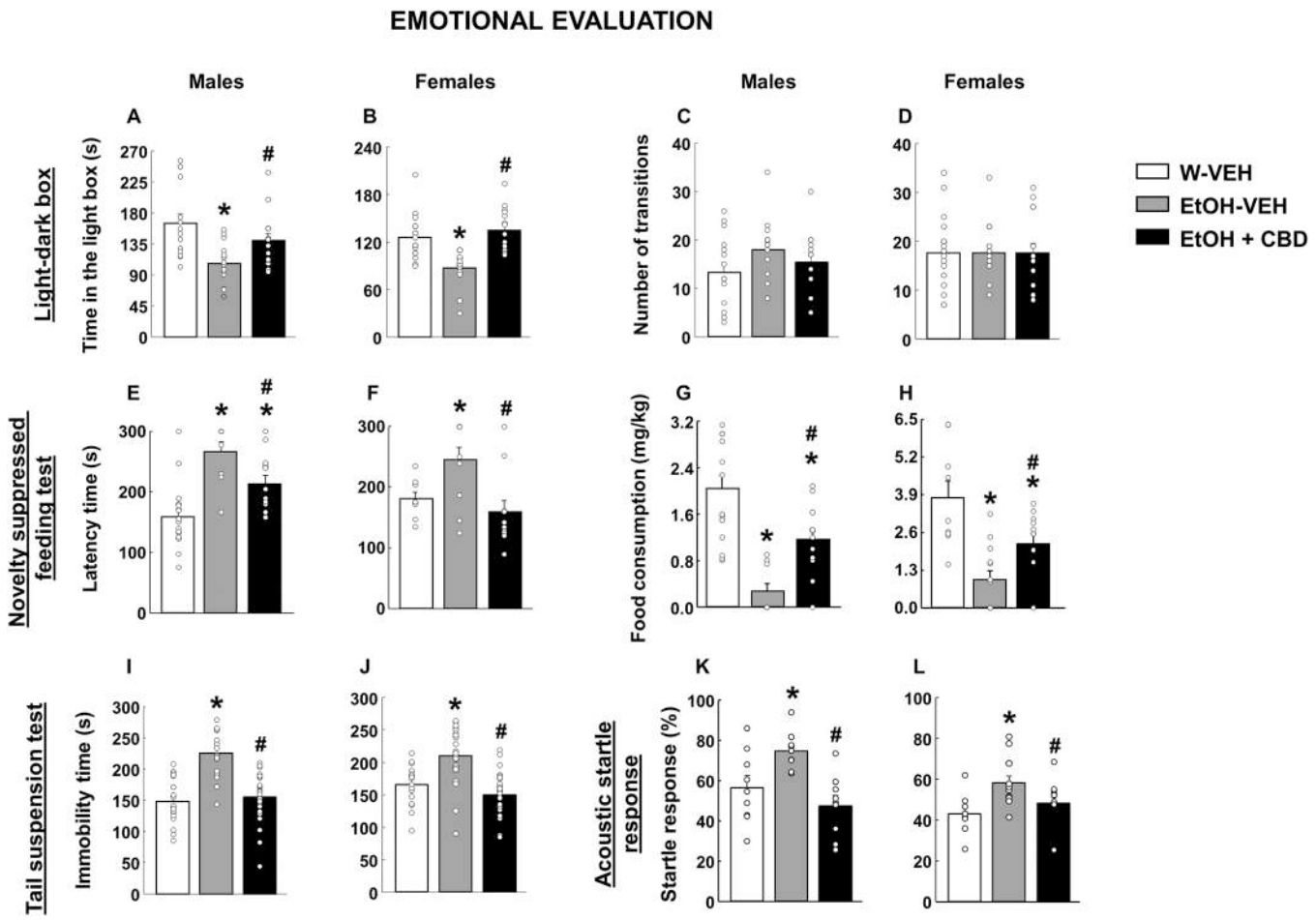

Fig. 2. Evaluation of the emotional alterations in male and female mice perinatally exposed to ethanol and chronically treated with CBD (30 mg/kg/24 h, i.p.). Immediately after weaning and for the next 5 weeks, mice were treated with CBD or VEH. From week 5 and during consecutive weeks until the end of the experiment, the emotional state of the mice and the effects of CBD were evaluated. Anxiety-like behaviors were analyzed by the light-dark box (time in the lighted box: A and B, number of transitions: C and D) and the latency time in the novelty-suppressed feeding (E and F) tests. Depressive-like behaviors were evaluated by the food consumption in the novelty-suppressed feeding (G and H) and tail suspension (I and J) tests. Emotional hyperreactivity was assessed by the acoustic startle response test (K and L). * $P < 0.05$ vs W-VEH group. # $P < 0.05$ vs EtOH-VEH group.

3.1.1.2. Novelty-suppressed feeding test (NSFT). In the NSFT paradigm, the results showed higher latency time in males (Fig. 2E, one-way ANOVA, $F(2,37)= 13.533$, $P < 0.001$) and females exposed to ethanol (Fig. 2F, one-way ANOVA, $F(2,32)= 6.896$, $P = 0.003$), and reduced food consumption (males, Fig. 2G, one-way ANOVA; $F(2,37)= 18.032$, $P < 0.001$; females, Fig. 2H, one-way ANOVA, $F(2,32)= 11.603$, $P < 0.001$) compared with controls. Chronic treatment with CBD normalized all these alterations in both sexes.

3.1.1.3. Tail suspension test (TST). Male and female mice exposed to the FASD model showed higher immobility time in the TST paradigm (males, Fig. 2I, one-way ANOVA, $F(2,61)= 24.729$, $P < 0.001$; females, Fig. 2J, one-way ANOVA, $F(2,68)= 18.542$, $P < 0.001$), compared to control samples. These changes were more pronounced in males than in females. CBD administration reduced this immobility time, reaching values similar to the W-VEH group in both sexes.

3.1.1.4. Acoustic startle response (ASR). Ethanol perinatal exposure increased the startle amplitude in males (Fig. 2K, one-way ANOVA, $F(2,26)= 8.145$, $P = 0.002$) and females (Fig. 2L, one-way ANOVA, $F(2,32)= 5.064$, $P = 0.013$). This effect was more pronounced in males than in females. The amplitude was normalized with CBD administration, reaching values similar to W-VEH groups in both males and females.

3.1.2. Cognitive evaluation

3.1.2.1. Novel object recognition (NOR). The discrimination index was reduced in males (Fig. 3A, one-way ANOVA, $F(2,65)= 4.452$, $P = 0.016$) and females (Fig. 3B, one-way ANOVA, $F(2,72)= 6.239$, $P = 0.003$) mice perinatally exposed to ethanol. However, CBD chronic administration increases this index, reaching values similar to those obtained in controls in males but not females.

3.1.2.2. Step-down inhibitory avoidance (SDIA). The results revealed reduced latency time in males (Fig. 3C, one-way ANOVA, $F(2,36)= 26.462$, $P < 0.001$) and females (Fig. 3D, one-way ANOVA, $F(2,28)= 5.255$, $P = 0.012$) perinatally exposed to ethanol in the 24 h evaluation. The chronic administration of CBD completely normalized these values in both sexes.

3.2. Gene expression analyses by RT-PCR

3.2.1. Stress-related targets

Relative gene expression analyses revealed an increased gene expression of *Crf* in the paraventricular nucleus (PVN) of males (Fig. 4B, one-way ANOVA, $F(2,26)= 15.844$, $P < 0.001$) and females (Fig. 4C, one-way ANOVA, $F(2,23)= 4.371$, $P = 0.026$) exposed to the FASD model. Also in this case, males were more affected than females. Interestingly, CBD normalized *Crf* gene expression in the PVN of males but

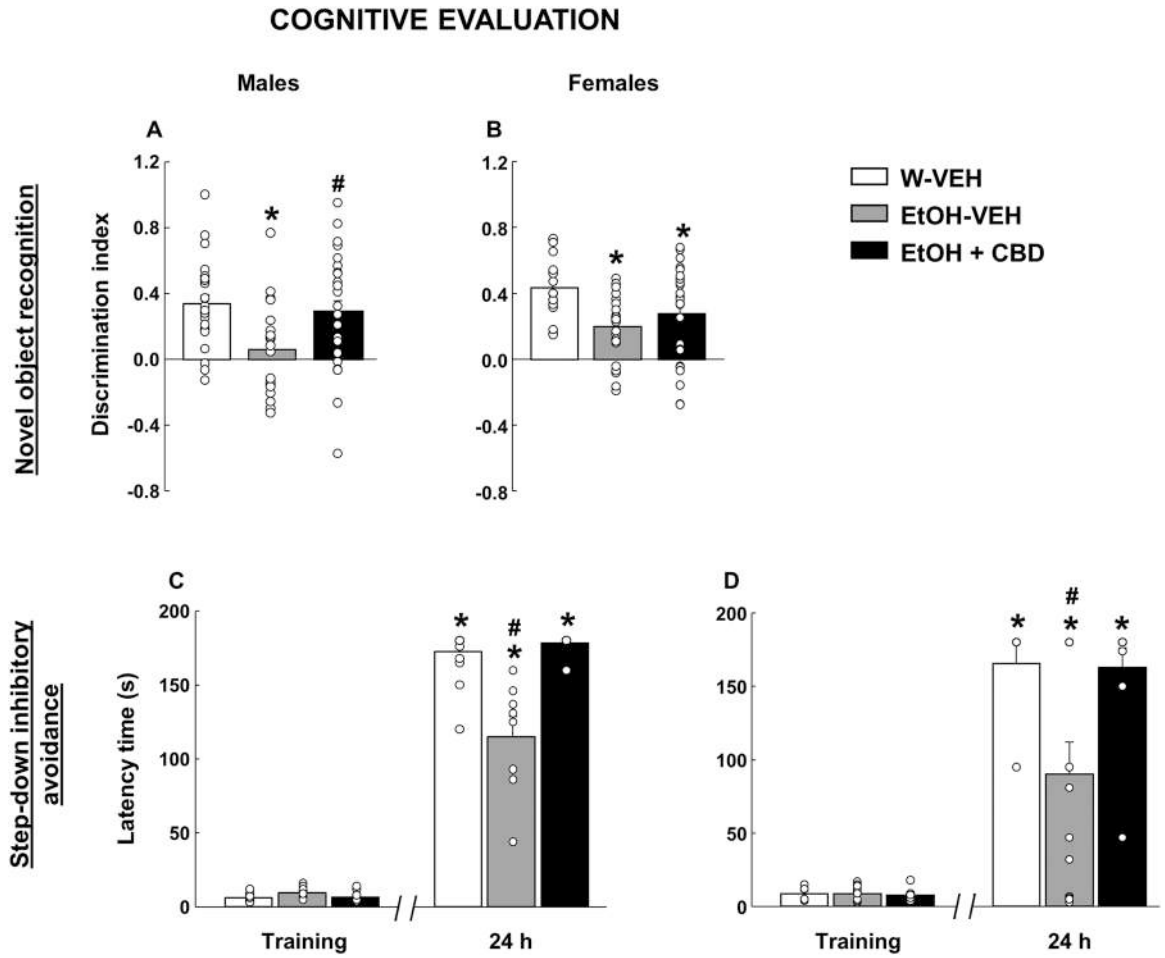

Fig. 3. Evaluation of the cognitive alterations in male and female mice perinatally exposed to ethanol and chronically treated with CBD (30 mg/kg/24 h, i.p.). Immediately after the weaning and during the following 5 weeks, mice were treated with CBD or VEH. Immediately after weaning and for the next 5 weeks, mice were treated with CBD or VEH. From week 5 and during consecutive weeks until the end of the experiment, the cognitive performance of the mice and the effects of CBD on its modulation were evaluated. The novel object recognition (A and B) and the step-down inhibitory avoidance (C and D) tests were used to assess recognition and emotional memories in mice. * $P < 0.05$ vs W-VEH group. # $P < 0.05$ vs EtOH-VEH group.

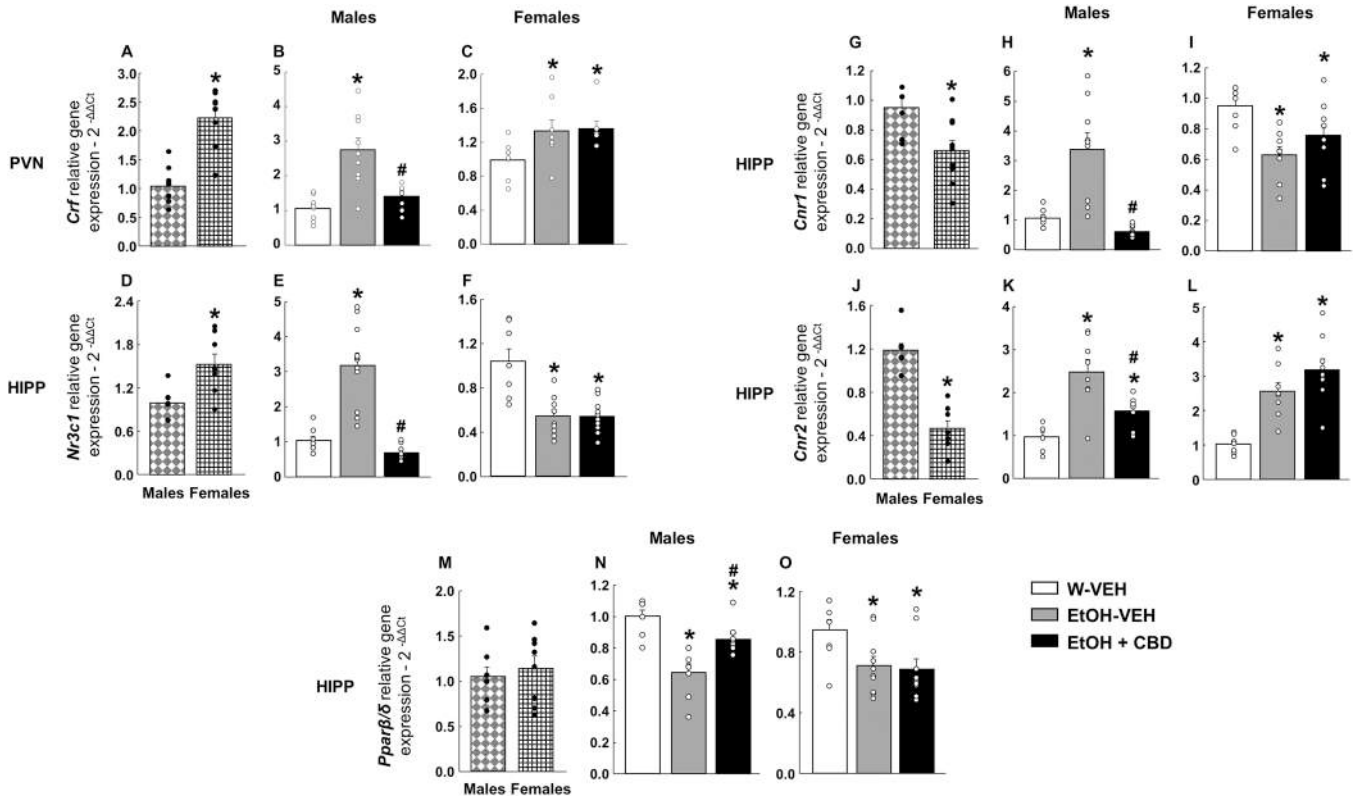

Fig. 4. Relative gene expression analyses by RT-PCR in male and female mice perinatally exposed to ethanol and chronically treated with CBD (30 mg/kg/24 h, i.p.). Corticotrophin releasing factor (Crf; A, B, and C) in the PVN and glucocorticoid receptor (Nr3c1; D, E, and F), cannabinoid receptors 1 (Cnr1; G, H, and I) and 2 (Cnr2; J, K, and L), and peroxisome proliferator-activated receptor β/δ (Pparβ/δ; M, N, and O) in the HIPP were analyzed. * $P < 0.05$ vs W-VEH or Males W-VEH group. # $P < 0.05$ vs EtOH-VEH group.

not in females. *Nr3c1* was analyzed as an additional target of the stress-axis regulation. Remarkably, male mice exposed to the FASD animal model showed increased relative gene expression of *Nr3c1* in the hippocampus (HIPP), which was reversed by chronic CBD administration (Fig. 4E, one-way ANOVA, $F(2,27)= 31.351$, $P < 0.001$). However, a reduction of *Nr3c1* gene expression was found in females, which was not normalized with CBD (Fig. 4F, one-way ANOVA, $F(2,27)= 15.584$, $P < 0.001$). Under basal conditions, females showed higher levels of *Crf* (Fig. 4A, Student's t-test, $t = -5.509$, $P < 0.001$, 14 d.f) and *Nr3c1* (Fig. 4D, Student's t-test, $t = -3.405$, $P = 0.004$, 14 d.f.), compared with males.

3.2.2. Endocannabinoid targets

Relative gene expression of the cannabinoid receptors *Cnr1* and *Cnr2* was analyzed in the HIPP. In male mice exposed to the FASD model, *Cnr1* gene expression was increased in the HIPP, which was normalized with chronic CBD administration (Fig. 4G, one-way ANOVA, $F(2,26)= 20.739$, $P < 0.001$). A significant increase in *Cnr2* gene expression was also found after the FASD model exposure, and CBD treatment tended to normalize the change (Fig. 4K, one-way ANOVA, $F(2,23)= 15.530$, $P < 0.001$). Interestingly, in females, a reduction of *Cnr1* (Fig. 4I, one-way ANOVA, $F(2,26)= 7.145$, $P = 0.004$) and an increase of *Cnr2* gene expressions were found in the HIPP (Fig. 4L, one-way ANOVA, $F(2,25)= 20.333$, $P < 0.001$). However, chronic CBD treatment did not normalize these changes. Under basal conditions, *Cnr1* (Fig. 4G, one-way ANOVA, Student's t-test, $t = 2.831$, $P = 0.012$, 16 d.f.) and *Cnr2* g gene expressions (Fig. 4J, Student's t-test, $t = 7.872$, $P < 0.001$, 14 d.f.) were reduced in the HIPP of females compared with males.

3.2.3. Pparβ/δ gene expression

The exposure to the FASD model significantly reduced the gene expression of *PPARβ/δ* in the HIPP of males (Fig. 4N, one-way ANOVA, $F(2,24)= 17.723$, $P < 0.001$) and females (Fig. 4O, one-way ANOVA, $F(2,27)= 4.588$, $P = 0.02$). Interestingly, CBD administration normalized the gene expression of *PPARβ/δ* in males but not in females. Under basal conditions, no differences were found between males and females in the expression of this gene (Fig. 4M, Student's t-test, $t = -0.512$, $P = 0.617$, 14 d.f.).

3.3. Conventional and confocal immunohistochemistry

3.3.1. Immunolabeling of NeuN, BDNF, NF200, and VGluT1 in DG and CA in the HIPP

In EtOH-VEH male mice, NeuN-immunostained sections observed at low magnification (Fig. 5A, B, C) revealed a decrease in the number of NeuN-ir cells in the CA_3 and the hilus of DG (double arrow in Fig. 5A, B, C) in EtOH-VEH samples, compared with W-VEH, and an increase in the male group treated with CBD. At a higher magnification, a decrease in the number of pyramidal cells in CA_3 areas was found in EtOH-VEH samples, compared with W-VEH, in male mice (arrow in Fig. 5 D, E). However, in male mice treated with CBD, a similar number of pyramidal NeuN-ir neurons in the CA_3 region and hilus were detected at low and higher magnifications, compared with W-VEH male mice (arrow Fig. 5A, C, D, F).

In female mice, we found a decrease in the NeuN-ir cells only in the CA_3 area in the EtOH-VEH group, but this effect was not as pronounced as in male mice (arrow in Fig. 6A, B, C). At higher magnification of the CA_3 region, a decrease in the number of pyramidal cells in CA_3 areas was found in EtOH-VEH, compared with W-VEH female mice (Fig. 6A, B, D, E). Similarly, to male mice, females treated with CBD showed a similar number of pyramidal NeuN-ir neurons in the CA_3 region, compared with W-VEH male mice, at both low and higher magnifications (Fig. 6A, C, D,

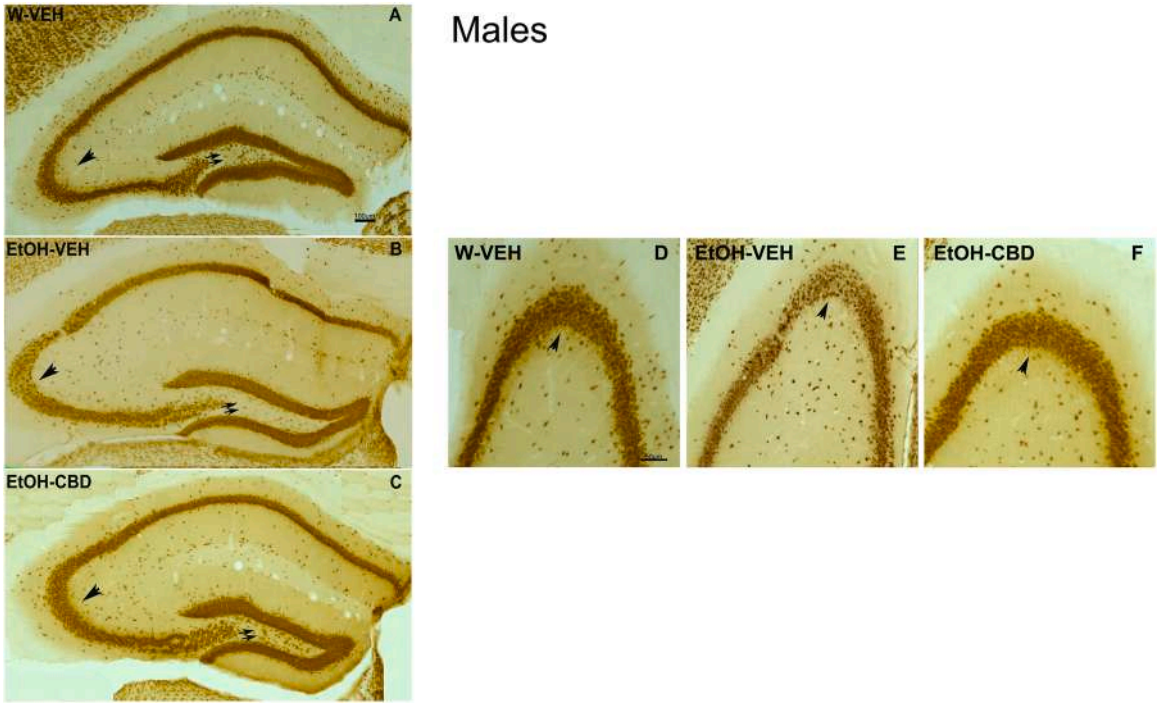

Fig. 5. Low magnification photomicrographs of NeuN-immunostained coronal sections of the hippocampus. Low magnification photomicrographs of coronal sections of the hippocampus showing NeuN-ir neurons in W-VEH, EtOH-VEH, and EtOH-CBD in male pups (A-C) at PND90. A decrease in the number of neurons in CA3 (arrow) and in DG (double arrow) was observed in EtOH-VEH (B) mice. Details of NeuN-ir neurons in CA3 (D-F) are shown. Note the decrease in de neuron numbers and labeling in this area in EtOH-VEH (B, E arrow) compared with W-VEH (A, E arrow) and EtOH-CBD (C, F arrow) male pups showed abnormal laminar organization of the hippocampus in EtOH-VEH pups and its recovery with EtOH-CBD.

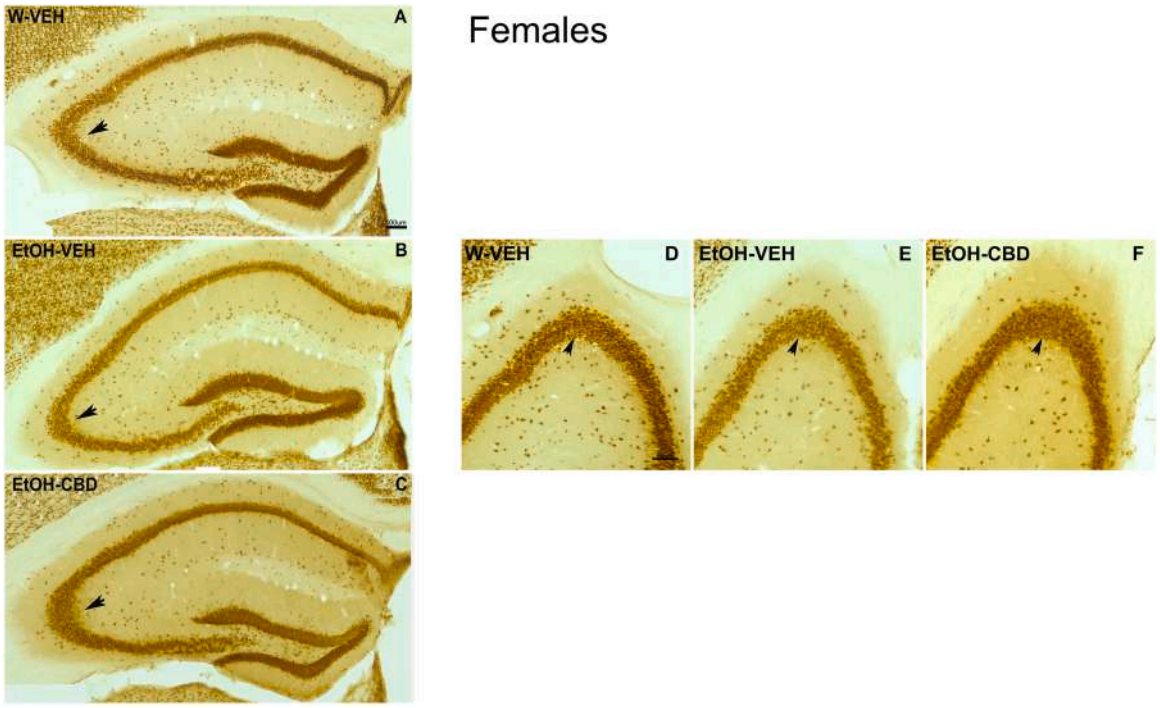

Fig. 6. Low magnification photomicrographs of NeuN-immunostained coronal sections of the hippocampus. Low magnification photomicrographs of coronal sections of the hippocampus showing NeuN-ir in neurons in W-VEH, EtOH-VEH, and EtOH-CBD in female pups (A-C) at PND60. Details of NeuN-in neurons in CA3 (D-F). Note the decrease in de neuron numbers and labeling in this area in EtOH-VEH (B, E arrow) compared with W-VEH (A, E arrow) and EtOH-CBD (C, F arrow) female pups showed abnormal laminar organization of the hippocampus in EtOH-VEH pups and its recovery with EtOH-CBD. Same scale for (A–C) and (D-F).

F). In both sexes, offspring showed an abnormal laminar organization of the HIPP in the EtOH-VEH groups and its recovery in the EtOH-CBD groups.

BDNF immunostaining revealed a lower labeling intensity of the cells in all HIPP areas in EtOH-VEH compared with W-VEH male mice, observed at low magnification (Fig. 7A, B). On the other hand, a decrease in the number and labeling intensity of BDNF-ir cells in the hilus and granular layer of DG (double arrow Fig. 7A, B, C), and the pyramidal layer of CA_1 and CA_3 was found in EtOH-VEH, compared with W-VEH and EtOH-CBD (Fig. 7A, B, C). The number of BDNF-immunostained pyramidal cells in CA_3 decreased in EtOH-VEH compared with W-VEH male mice and increased in EtOH-CBD mice (arrowhead in Fig. 7A, B, C). Likewise, BDNF-ir cells in the hilus and granular BDNF-ir cells in the DG areas (double arrow Fig. 7A, B, C) were decreased. At high magnification, BDNF-ir cells in the pyramidal area of the CA_3, the hilus, and the granular cells of DG in the EtOH-CBD group increased compared with EtOH-VEH male mice (Fig. 7 D, E, F, G, H, I).

Even though BDNF-immunostained intensity is higher in EtOH-VEH female mice than in male mice, the BDNF immunostaining showed a lower labeling intensity in EtOH-VEH female group compared with W-VEH and EtOH-CBD female mice (Fig. 8A, B, C). At high magnification, pyramidal BDNF-ir cells decreased in EtOH-VEH female mice and increased in the group of females treated with CBD, compared with W-VEH female mice (arrowhead in Fig. 8 D, E, F). The labeling intensity was reduced in EtOH-VEH females and increased in EtOH-CBD, compared with W-VEH female mice in the granular cells of the DG in the HIPP (double arrow in Fig. 8G, H, I). All these results reveal increased cell survival and plasticity in EtOH-CBD, compared with EtOH-VEH, in male and female mice.

The immunohistochemistry assay for NF-200 showed decreased NF200-ir in all HIPP areas in EtOH-VEH, compared to W-VEH, and its recovery in EtOH-CBD in male mice (Fig. 9A, B, C). Notably, the decrease in NF200-ir of CA_3 strata lucidum and radiatum, in the CA_1 stratum lacunosum-moleculare (arrow in Fig. 9A, B), and the hilus of DG (double arrow Fig. 9A, B) were more pronounced in the EtOH-VEH group, compared with W-VEH male mice. Interestingly, the N200-ir intensity increased in the group treated with CBD, compared with EtOH-VEH male mice, achieving an intensity similar to that of the W-VEH group (Fig. 9A, B, C). At a high magnification of the hilus in the DG, the NF200-ir was lower in the EtOH-VEH than in W-VEH male mice. Note the recovery in the EtOH-CBD male group (Fig. 9 D, E, F).

In female mice, a decreased NF200-ir was found in CA_3 strata lucidum and radiatum, CA_1 stratum lacunosum-moleculare (arrow Fig. 10A, B), and in the hilus of DG (double arrow Fig. 10A, B) in EtOH-VEH mice, compared to W-VEH. Also, an increase in NF200-ir cells was detected in the females treated with CBD, compared with EtOH-VEH, being the immunostained similar to that of the W-VEH group (Fig. 10A, B, C). At high magnification, NF200-ir in the hilus of the DG was lower in EtOH-VEH than in W-VEH and EtOH-CBD female mice. At high magnification, NF200-ir was similar in the EtOH-CBD group and the W-VEH group and higher than in EtOH-VEH female mice in the hilus of the DG (Fig. 10 D, E, F). These data reveal an alteration of the stabilization and maturation of connections in the EtOH-VEH group, compared to W-VEH and the normalization of these effects with the early and chronic treatment with CBD in male and female mice.

Low-power confocal micrographs (Fig. 11A, B, C and Fig. 12A, B, C) showed that the distribution of VGluT1-ir boutons in CA_3 and CA_1 from EtOH-VEH male and female mice was abnormal. These results revealed an alteration of the laminar distribution of excitatory input. In EtOH-VEH male mice, the VGluT1-ir bouton was decreased in strata oriens, lucidum and radiatum of CA_3 (double arrows in Fig. 11 B) and stratum lacunosum-moleculare of CA_1, in comparison to W-VEH male mice (arrow in Fig. 11. A, B). In particular, the area occupied by VGluT1-ir boutons (mossy boutons) in strata oriens and lucidum of CA_3 was lower than in W-VEH male mice (double arrows Fig. 11A, B, D, E).

However, an increase in the area occupied by VGluT1-ir mossy boutons was found in the strata lucidum of EtOH-CBD female offspring, compared with the EtOH-VEH group (double arrow in Fig. 11A, B, C, D,

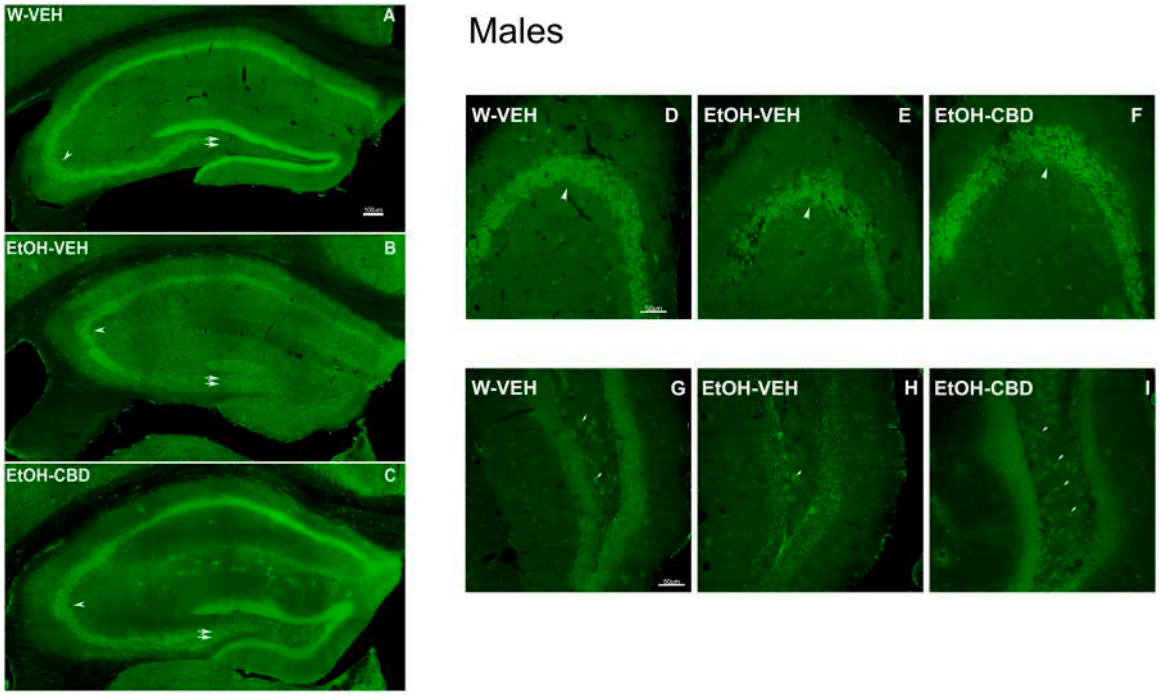

Fig. 7. Low magnification confocal images showing altered immunolabeling of BDNF in ETOH-VEH2 male pups. Collages of confocal photomicrographs showing BDNF-ir (green labeling; A-C), in the hippocampus of W-VEH (A), EtOH-VEH (B), and EtOH-CBD (C) pups at PND60. Details of BDNF-in cells in DG (D-F) and CA3 (G-I). Note the decrease in the number and immunostained of BDNF-ir cells in the hilus and granular layer of DG and the pyramidal layer of CA1 and CA3, in EtOH-VEH (A-B-H) in male pups compared with W-VEH (B, D, G) and EtOH-CBD (C, F, I). Showing an increase in cell survival and plasticity in EtOH-CBD compared with EtOH-VEH male pups. Same scale for (A–C) and (D-I).

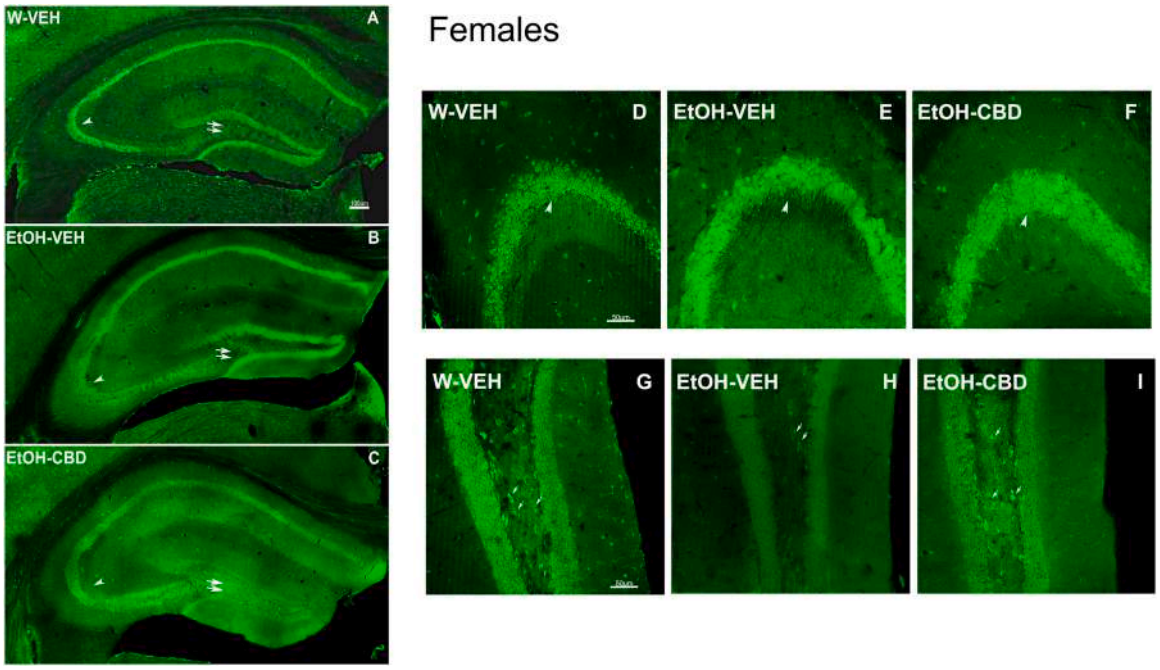

Fig. 8. Low magnification confocal images showing altered immunolabeling of BDNF in EtOH-VEH2 female pups. Collages of confocal photomicrographs showing BDNF-ir (green labeling; A-I), in the hippocampus of W-VEH (A), EtOH-VEH (B), and EtOH-CBD (C) pups at PND60. Details of BDNF-in cells in DG (D-F) and CA3 (G-I). Note the decrease in the number and labeling of BDNF-ir cells in the hilus and granular layer of DG and the pyramidal layer of CA1 and CA3, in EtOH-VEH (A-B-H) in male pups compared with W-VEH (B, D, G) and EtOH-CBD (C, F, I). Showing an increase in cell survival and plasticity in EtOH-CBD compared with ETOH-VEH female pups. Same scale for (A–C) and (D-I).

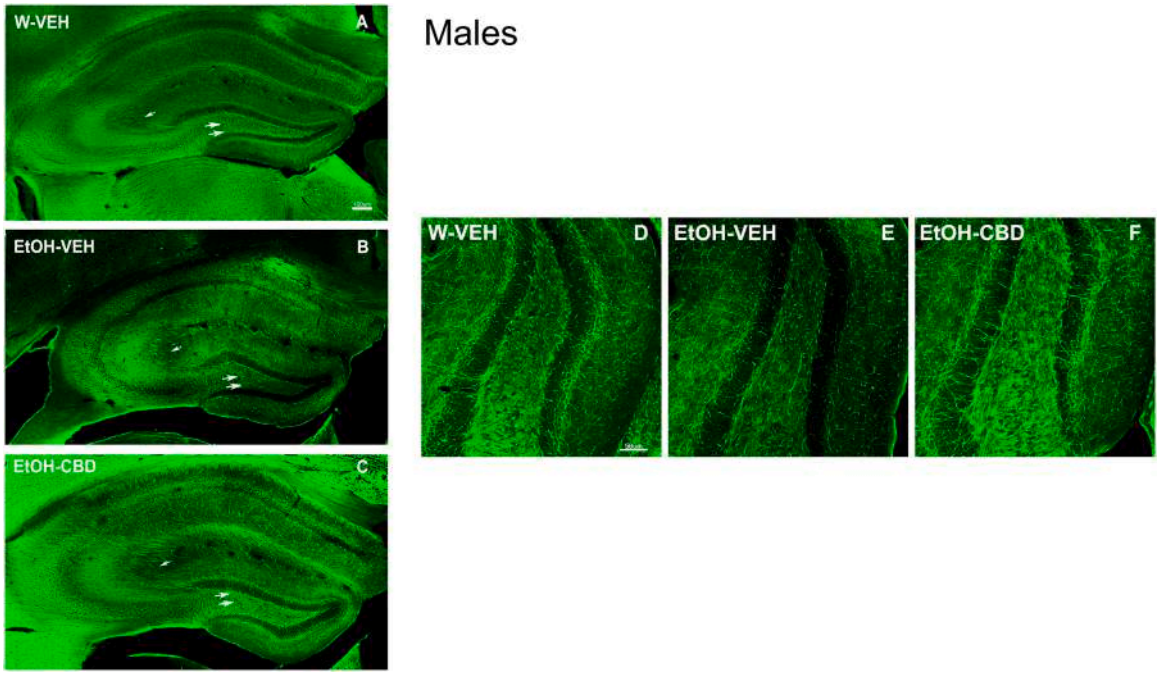

Fig. 9. Low magnification confocal images showing abnormal immunolabeling of NF200 in EtOH-VEH2 male pups. Confocal photomicrographs showing NF200-ir (green labeling; A-F), in the hippocampus of W-VEH (A), EtOH-VEH (B), and EtOH-CBD (C) pups at PND60. Note the decreased NF200-ir in CA3 strata lucidum (double arrow) and radiatum, in the CA1 stratum lacunosum-moleculare (arrow) and the hillus of DG in EtOH-VEH (B) compared to W-VEH (A) and its recovery in EtOH-CBD (C) male mice. Magnification of the hilus of the DG, the NF200-ir cells is less in EtOH-VEH (E) male mice than in W-VEH group (D). Note the recovery in EtOH-CBD pups (F). These data show an alteration in the stabilization and maturation of connections in EtOH-VEH (E) pups compared to W-VEH (D) and the CBD normalizes it. Same scale for (A-C) and (D-F).

E, F). In female mice, although it was not as pronounced as in males, the VGluT1-ir bouton in EtOH-VEH was decreased in strata oriens, lucidum and radiatum of CA3 (double arrows in Fig. 12A, B, C) and stratum lacunosum-moleculare of CA_1 in comparison to W-VEH female mice (arrow in Fig. 12A, B). The area occupied by VGluT1-ir boutons (mossy boutons) in strata oriens and lucidum in the EtOH-VEH group of CA_3 was

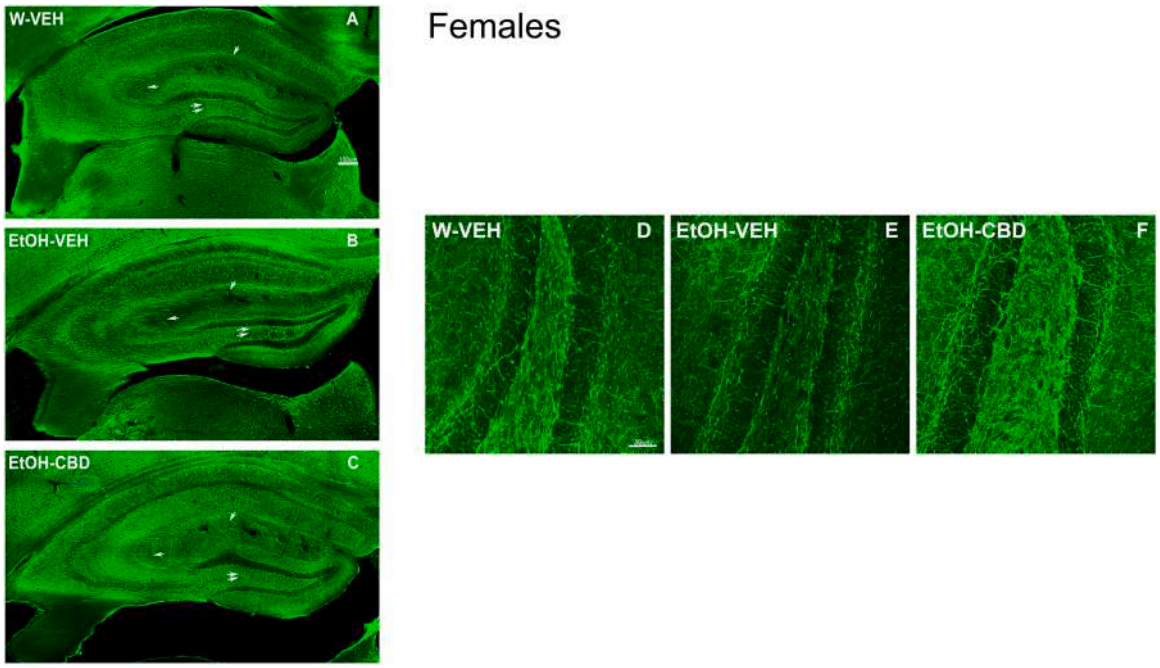

Fig. 10. Low magnification confocal images showing abnormal immunolabeling of NF200 in EtOH-VEH2 female pups. Confocal photomicrographs showing NF200-ir (green labeling; A-F), in the hippocampus of H2O-VEH (A), ETOH-VEH (B), and ETOH-CBD (C) pups at PND60. Note the decreased NF200-ir in CA3 strata lucidum (double arrow) and radiatum, in CA1 stratum lacunosum-moleculare (arrow) and the hilus of the DG in EtOH-VEH (B) compared to W-VEH (A) and its recovery in EtOH-CBD (C) group. Magnification of the hilus of DG the NF200-ir is less in EtOH-VEH (E) pups than in W-VEH pups (D). Note the recovery in EtOH-CBD pups (F). These data show an alteration in the stabilization and maturation of connections in EtOH-VEH (E) pups compared to W-VEH (D) and the CBD normalizes it. Same scale for (A–C) and (D-F).

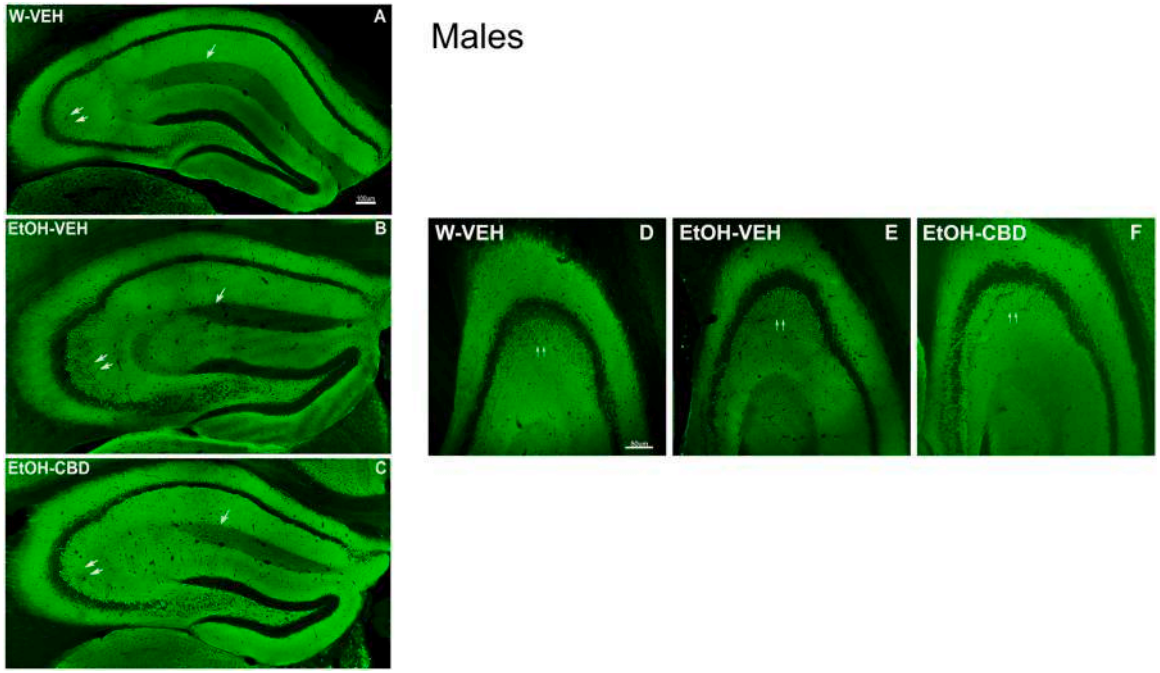

Fig. 11. Low magnification confocal images showing abnormal immunolabeling of VGLUT-1 in EtOH-VEH2 male pups. Collages of confocal photomicrographs showing VGluT1-ir (green labeling; A-F), in the hippocampus of W-VEH (A), EtOH-VEH (B), and EtOH-CBD (C) pups at PND60. Note the decreased VGluT1-ir in CA3 strata lucidum (double arrow) and radiatum, and CA1 stratum lacunosum-moleculare (arrow) in EtOH-VEH (B) compared to W-VEH (A) and its recovery in EtOH-CBD (C) pups. Magnification of the area occupied by VGluT1-ir mossy boutons in the strata lucidum (arrow D-F) of CA3 is less in EtOH-VEH (E) pups than in W-VEH pups (D). Note the increase in the area occupied by VGluT1-ir mossy boutons in the strata lucidum of EtOH-CBD pups compared with the EtOH-VEH group (F). These data show an alteration of the laminar distribution of excitatory inputs in EtOH-VEH pups compared to W-VEH and the CBD normalizes the normal excitatory distribution. Same scale for (A–C) and (D-F).

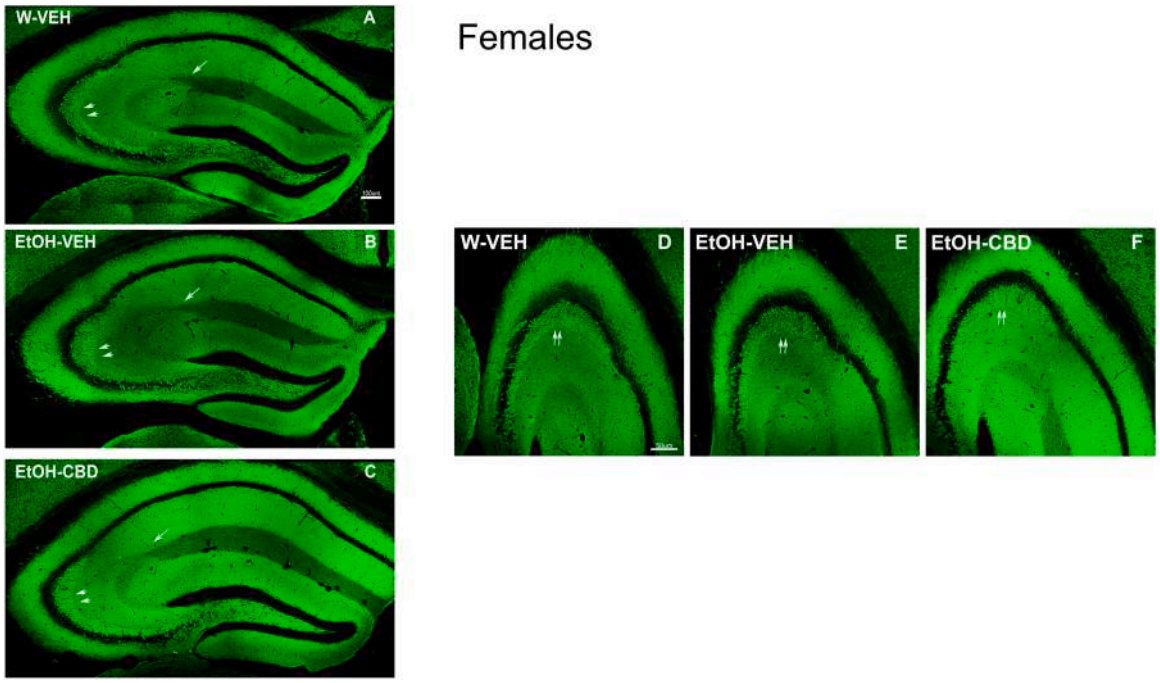

Fig. 12. Low magnification confocal images showing abnormal immunolabeling of VGLUT-1 in ETOH-VEH2 female pups. Collages of confocal photomicrographs showing VGluT1-ir (green labeling; A-F), in the hippocampus of W-VEH (A), EtOH-VEH (B), and EtOH-CBD (C) pups at PND60. Note the decreased VGluT1-ir in CA3 strata lucidum (double arrow) and radiatum, and CA1 stratum lacunosum-moleculare (arrow) in EtOH-VEH compared to W-VEH and its recovery in EtOH-CBD pups. Magnification of the area occupied by VGluT1-ir mossy boutons in the strata lucidum (arrow D-F) of CA3 is less in EtOH-VEH (E) pups than in W-VEH pups (D). Note the increase in the area occupied by VGluT1-ir mossy boutons in the strata lucidum of EtOH-CBD pups compared with the EtOH-VEH group (F). These data show an alteration of the laminar distribution of excitatory inputs in EtOH-VEH pups compared to H2O-VEH and the CBD normalizes the excitatory distribution. Same scale for (A-F) and (D-F).

lower than in W-VEH female mice (double arrows Fig. 12A, B, D, E). However, at high magnification, an increase in the area occupied by VGluT1-ir mossy boutons was found in the strata lucidum of EtOH-CBD female pups compared with the EtOH-VEH group (arrow in Fig. 12 B, C). These results revealed that CBD administration normalizes the excitatory distribution in male and female perinatally ethanol-exposed mice (double arrow in Fig. 11 D, E, F and Fig. 12 D, E, F).

3.4. Targeted metabolomics

The metabolomics results showed that the treatment with EtOH and EtOH-CBD induces significant changes in the metabolic profiles of the HIPP of both male and female mice. However, this effect was reduced in the PFC, especially in female mice (Fig. 13A). The metabolic differences between the experimental groups were verified when the same data set were analyzed using heat maps (Fig. 13B).

Further analyses of the results using IPA, revealed significant differences on the main canonical pathways that are predicted to be affected in each of the groups (Fig. 14A-B). The same was the case for the primary diseases and functions expected to be differently affected (Fig. 14C). CBD has multiple cellular targets in mammals, including some mitochondrial ones, such as the regulation of the oxidative status of the cells [45,46]. However, the targeted metabolomics assay did not show significant differences in the main mitochondrial pathways in the FASD model (Figs. 13 and 14).

4. Discussion

The results of this study reveal that the early and chronic administration of CBD significantly improves the behavioral and neurobiological alterations found in mice exposed to a model of FASD. The following points support this statement: (1) male and female mice perinatally exposed to ethanol showed significant anxiogenic and depressive-like behaviors and emotional hyperreactivity that were restored with the CBD administration; (2) mice also showed cognitive disturbances that were modulated with CBD in males but not in all the tests in females; (3) these behavioral changes were accompanied with gene expression alterations in different brain targets (*Crf*, *Nr3c1*, *Cnr1*, *Cnr2,* and *Pparβ/δ)*, that were normalized with CBD administration in males but not in females; (4) mice exposed to the FASD model showed cellular alterations in the number of cells, neurofilaments, neuroplasticity and glutamatergic neurotransmission in the HIPP, that were repaired in males and females treated with CBD; and (5) metabolomic pathways involved in purine ribonucleosides degradation to ribose-1-phosphate, sirtuin signaling pathway, purine nucleotides degradation (aerobic), NAD biosynthesis (from tryptophan), phenylalanine degradation, and ferroptosis signaling, that were modulated with CBD. Interestingly, no significant alterations were detected in mitochondrial targets, including OXPHOS, in any of the groups.

Several animal models have been developed to simulate FASD and elucidate the molecular and behavioral alterations underlying these disorders. The experimental procedures used in these models vary considerably, exposing female pregnant rodents or offspring to different concentrations of alcohol by oral gavage or subcutaneous administration in different stages of the gestational or postnatal periods [21, 47–55]. The FASD model used in this study has included some specific features that may differentially modify the results found compared with previously published models. Firstly, female mice were exposed to the voluntary alcohol consumption paradigm, and after reaching the higher concentration of ethanol and stabilization 10%, only the animals with a higher preference for ethanol (73.8%) and consumption (9.4 g/kg) were selected to cross them (Supplementary Figure 1). This approach allows for simulating the previous alcohol consumption history in females. To our knowledge, this is the first study considering this previous alcohol consumption for developing the animal model of FASD. Secondly, after crossing with a male and between GD7 and the pup's weaning at PND21,

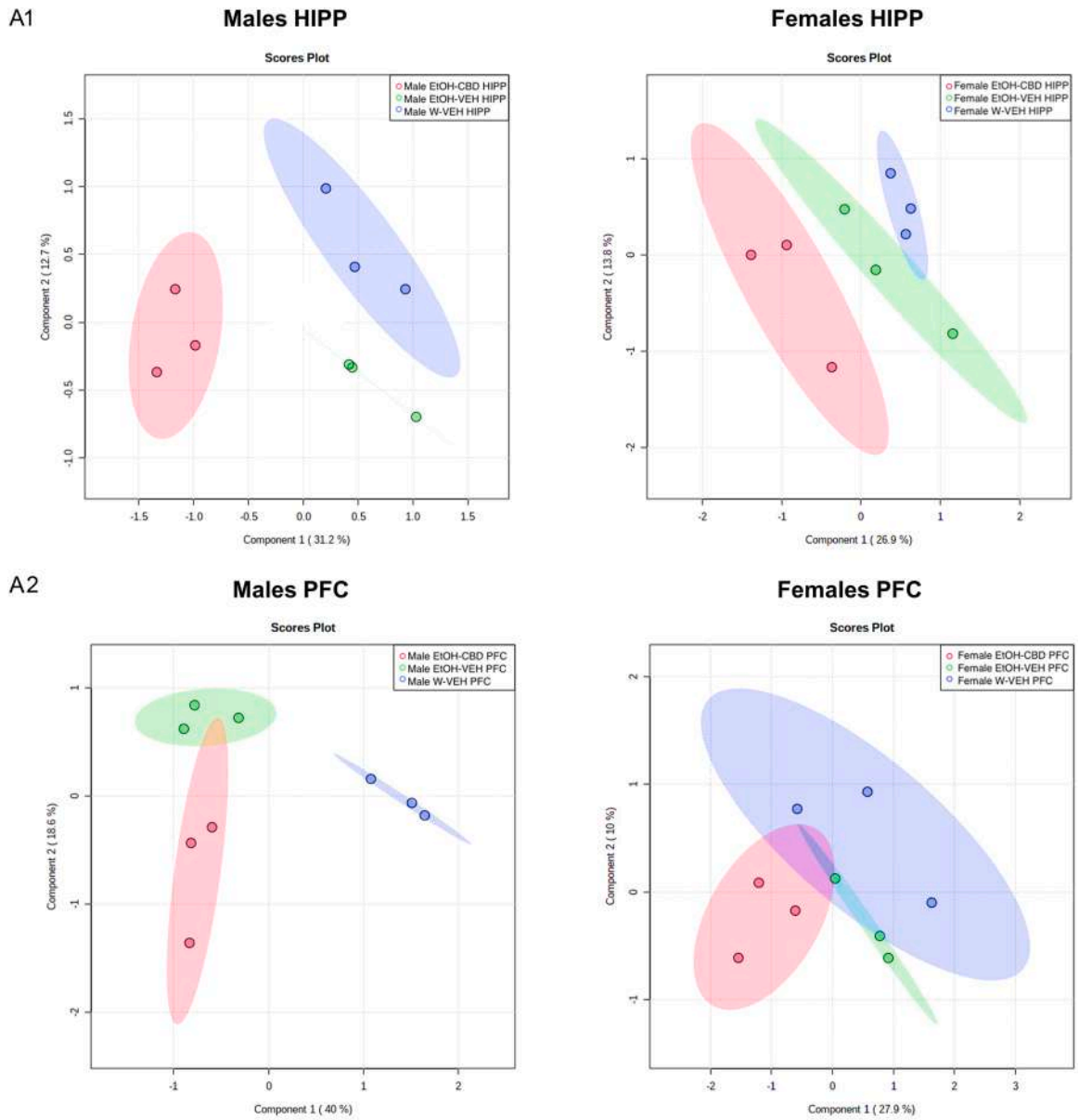

Fig. 13. Metabolomic analysis shows clear differences between the experimental groups included in this study. A. Principal Component Analysis (PCA) shows that HIPPs have different metabolomics profiles. However, in the case of PFCs, and especially in the case of females within this group, there is some overlapping between the metabolomic profile of the different experimental conditions. Shaded areas show regions with at least 95% of confidence (p-value ≤ 0.05). B. Heat maps showing the top 30 metabolites whose presence is more significantly different in each of the experimental groups. Red colors represent metabolites that are upregulated, while blue shows downregulation (p-value ≤ 0.05).

females received 3 mg/kg of ethanol by oral gavage twice a day, simultaneously maintaining the bottles for voluntary ethanol consumption. Maintaining the bottles was to avoid any abstinence period in females between both gavage administrations.

Interestingly, the voluntary ethanol consumption using these bottles was completely null, indicating the absence of abstinence periods. One hour after the last ethanol administration, it is relevant to mention that ethanol concentrations in the plasma were significantly elevated (179.02 ± 20.16 mg/dl) causing some problems in the motor coordination of females [21,53]. These were noticed especially at the beginning of the ethanol gavage administration and diminished throughout treatment. Both aspects suggest that despite administering ethanol twice a day, offspring were exposed to stable alcohol concentrations, contributing to the induction of long-lasting and noticeable behavioral and neurobiological alteration.

On the weaning day, the daily offspring administration of CBD started at a dose of 30 mg/kg (i.p.) to evaluate if the early and chronic administration of this drug could modulate some of the model-induced alterations that were evaluated between PND56–91 (Fig. 1). A significant sex-dependent anxiety and depressive-like behaviors were found in male and female offspring exposed to the animal model of FASD. Both males and females showed higher anxiogenic and depressive-like behaviors in the LDB, NSFT, TST, and ASR. It is relevant to mention that males were more affected by the PEA protocol exposure than females (Fig. 2). Both male and female mice also showed cognitive impairments in the recognition and aversive memories retention evaluated by the NOR and SDIA tests (Fig. 3). These sex-dependent differences could be associated with different vulnerability to ethanol actions during the gestational and lactational periods, as previously reported in other animal models of PAE [47,56,57]. Simultaneously, the chronic

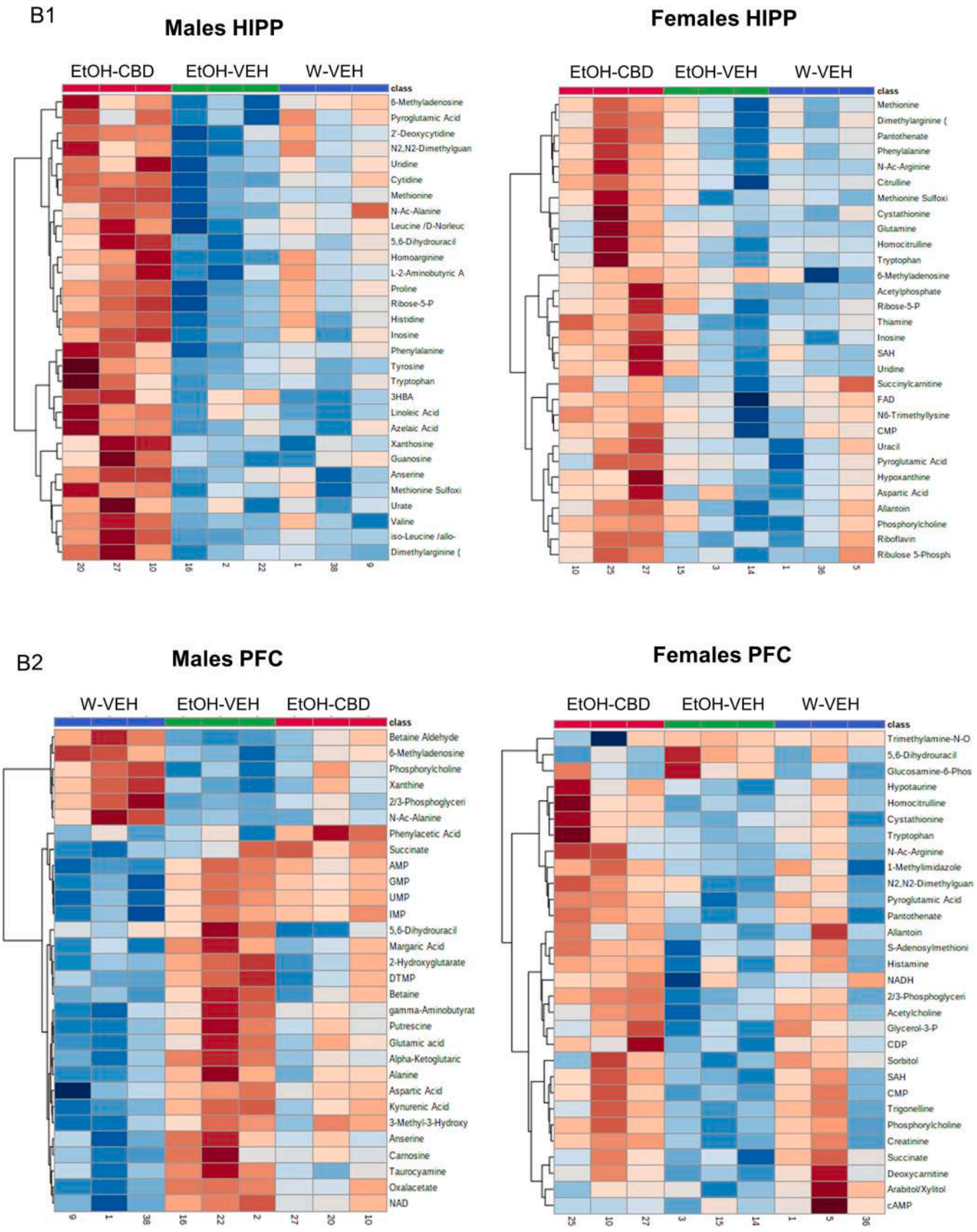

Fig. 13. (*continued*).

A1

HIPP
EtOH-VEH vs. W-VEH

Males

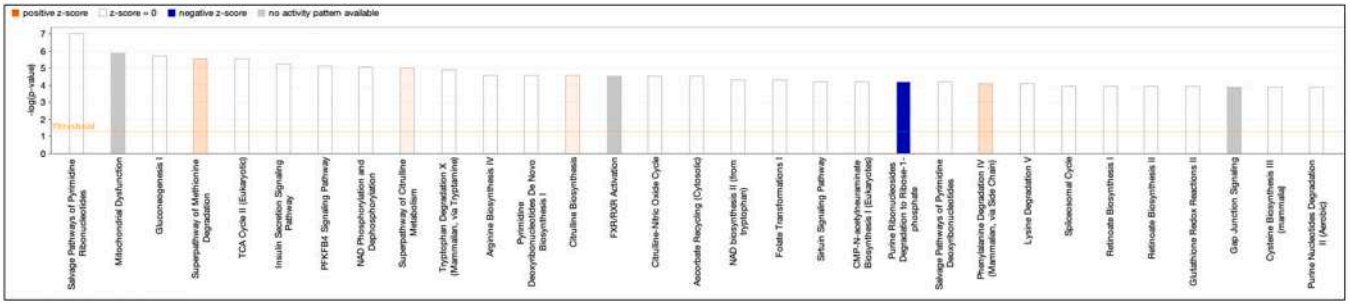

Females

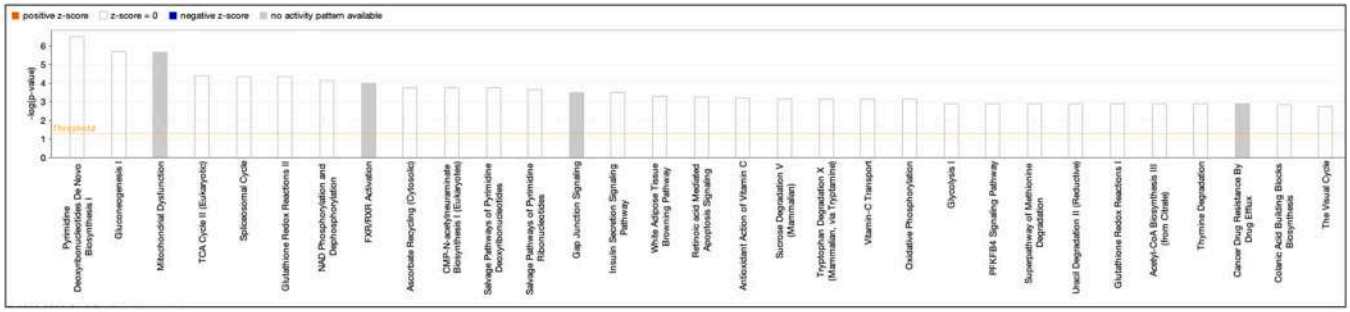

A2

PFC
EtOH-VEH vs. W-VEH

Males

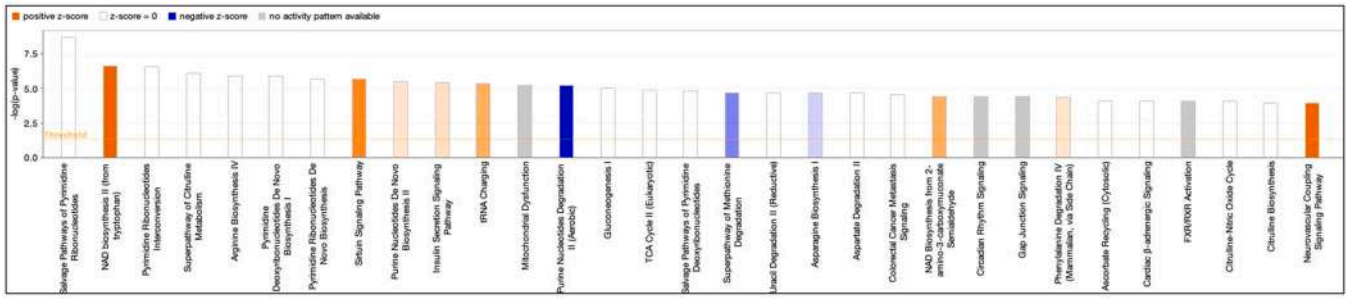

Females

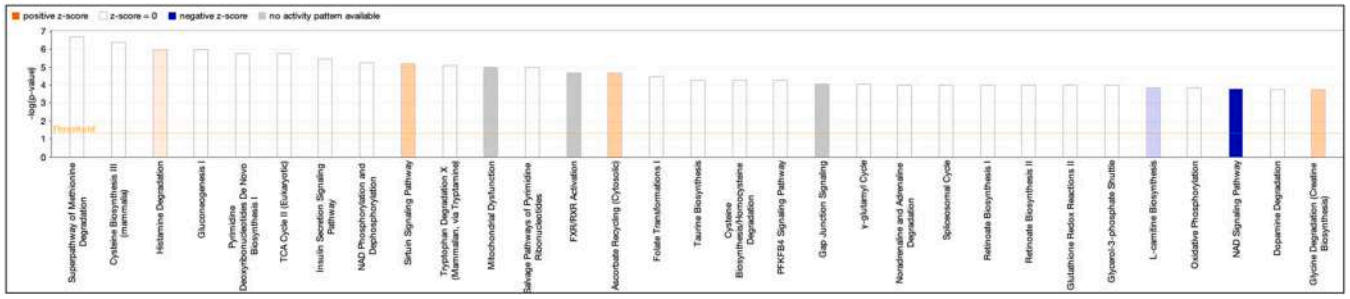

Fig. 14. IPA predicts differences in the canonical pathways and the diseases and functions affected by CBD, and CBD and EtOH in the different experimental groups. A. Graphs showing the main differentially affected canonical pathways predicted in samples treated with ethanol, when compared with the control samples. Canonical pathways were identified using IPA based on metabolites. In this case, the p-value was set at 0.5, which allowed us to select between 200 and 300 metabolites per experimental group. The bars represent the significance of each of the canonical pathways. Specifically, we show the 31 one pathways that IPA predicted with the highest statistical power in each of the experimental groups. Canonical pathways which are likely activated are presented in orange (positive z-score), while those pathways that are likely inhibited are presented in blue (negative z-score). B. Graphs showing further analysis of the obtained data regarding the canonical pathways.

Specific pathways were selected considering the most affected according to the analyses conducted in IPA. To conduct a comparison between these pathways in the treated groups, and not exclusively between each independent group and the controls, we used the following formula for each of the experimental groups: [-log (p-value) W-VEH vs. EtOH-CBD] - [-log (p-value) W-VEH vs. EtOH-VEH]. C. Graphs representing the main diseases and functions that are predicted to be affected in our samples. In this case, we used the same approach as in B to obtain these values.

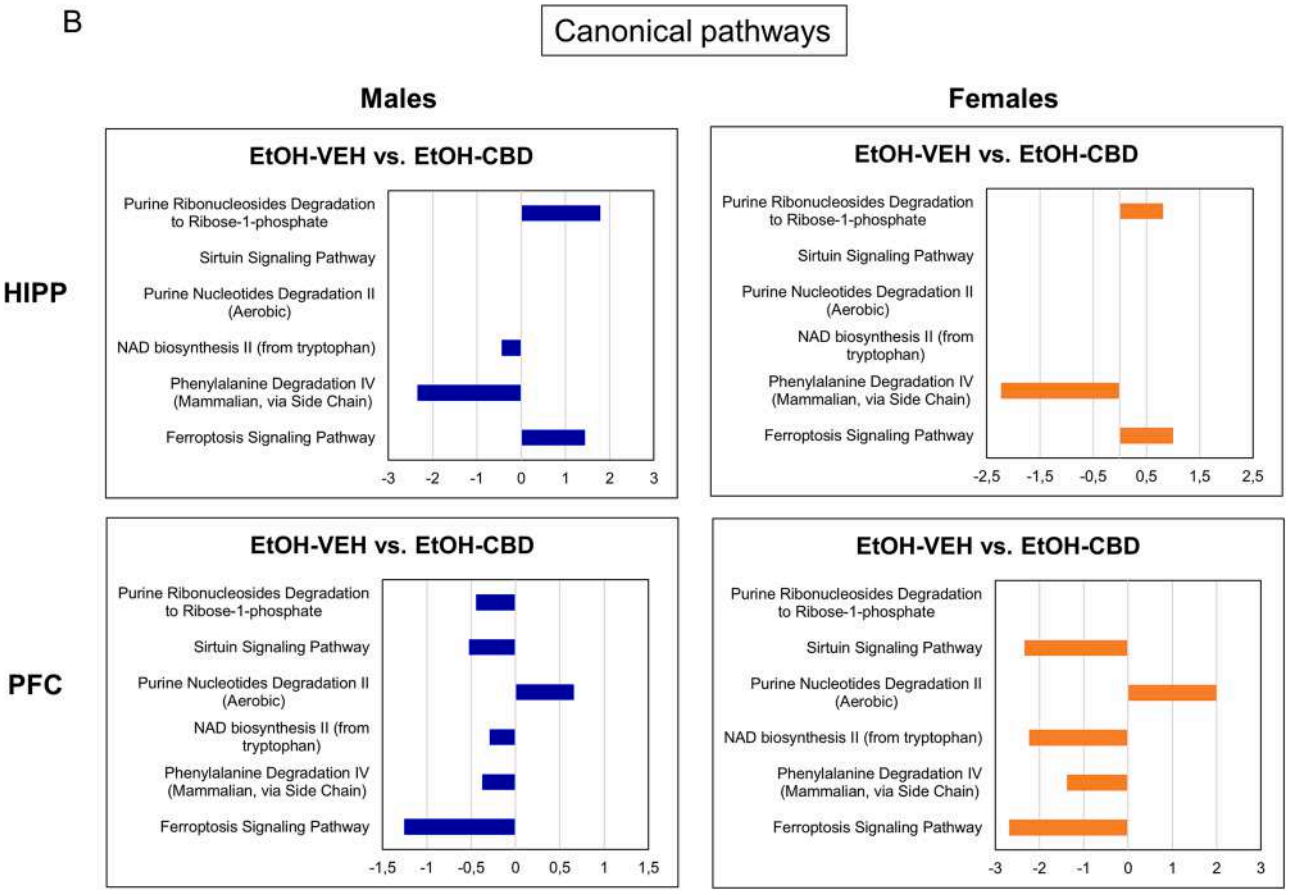

Fig. 14. (*continued*).

administration of CBD starting at PND21 repaired these anxiogenic and depressive-like alterations in the LDB, NSFT, TST, and ASR tests in males and females. Significant sex-dependent differences were found by evaluating cognitive alterations by NOR and SDIA tests. Specifically, the treatment with CBD normalized the cognitive alterations in the NOR and SDIA tests in males. However, it did not modulate the cognitive deficits in females nor the NOR test (Fig. 3). To date, only one study evaluated the potential usefulness of CBD in an animal model of FASD by administering this drug to ethanol-exposed offspring between PND25 and 34 [21]. The results of the present study are consistent with those reported by García-Baos and colleagues regarding the usefulness of CBD in modulating these cognitive aspects. However, in the present study, sex-dependent differences in CBD's actions were also found, which was not previously reported. Furthermore, no preclinical studies evaluating CBD utility in modulating FASD model-induced emotional disturbances were described (Fig. 2). To our knowledge, this is the first animal study revealing that early and chronic CBD administration normalizes FASD model-induced anxiety, depressive-like behaviors, and emotional hyperreactivity, suggesting the potential usefulness of this drug in the pharmacological management of patients with FASD.

Different experimental methods such as gene and protein expressions, immunohistochemistry and metabolomics were carried out to explore the neurobiological mechanisms underlying CBD's behavioral actions. As main regulatory targets of the hypothalamic-pituitary-adrenal (HPA) axis activity, the relative gene expression of *Crf* and *Nr3c1* in the PVN and HIPP, respectively, were evaluated to explain the molecular bases of the emotional and cognitive alterations induced by the FASD model, and to explore the potential mechanisms by which CBD could reverse these changes. The exposure to the PAE protocol increased *Crf* relative gene expression in male and female offspring, consistent with the emotional alterations observed in these mice. Indeed, higher anxiety-like behaviors are associated with increased *Crf* gene expression. Under basal conditions, *Crf* gene expression in females was increased compared with males, which aligns with a previous study [58]. No information about the alterations in the HPA axis is available in mice exposed to ethanol during their perinatal period. Under normal stress-axis functioning, increased *Crf* levels in the PVN are accompanied by reduced levels of *Nr3c1* in the HIPP, consistent with the results found in female offspring exposed to the FASD model (Fig. 4C and F). However, different experimental conditions, such as exposure to an adverse situation in the perinatal period or early adolescence, could alter this normal HPA axis negative feedback, resulting in elevated *Nr3c1* mRNA levels even in the presence of increased *Crf* gene expression [26].

Interestingly, CBD administration normalized *Crf* and *Nr3c1* gene expressions in males, achieving values similar to those in control samples. However, it did not modify the changes in females (Fig. 4). These sex-dependent CBD effects were reported previously in other experimental conditions. For example, in a binge alcohol drinking model, the dose of CBD to reduce alcohol intake in males did not modulate alcohol consumption in females, requiring a higher dose to reach the same effect than in males [59]. Thus, it could be hypothesized that the inefficacy in modulating HPA axis-related alterations in females could be related to the dose selected for this study.

CBD presents a multimodal mechanism of action, acting on more

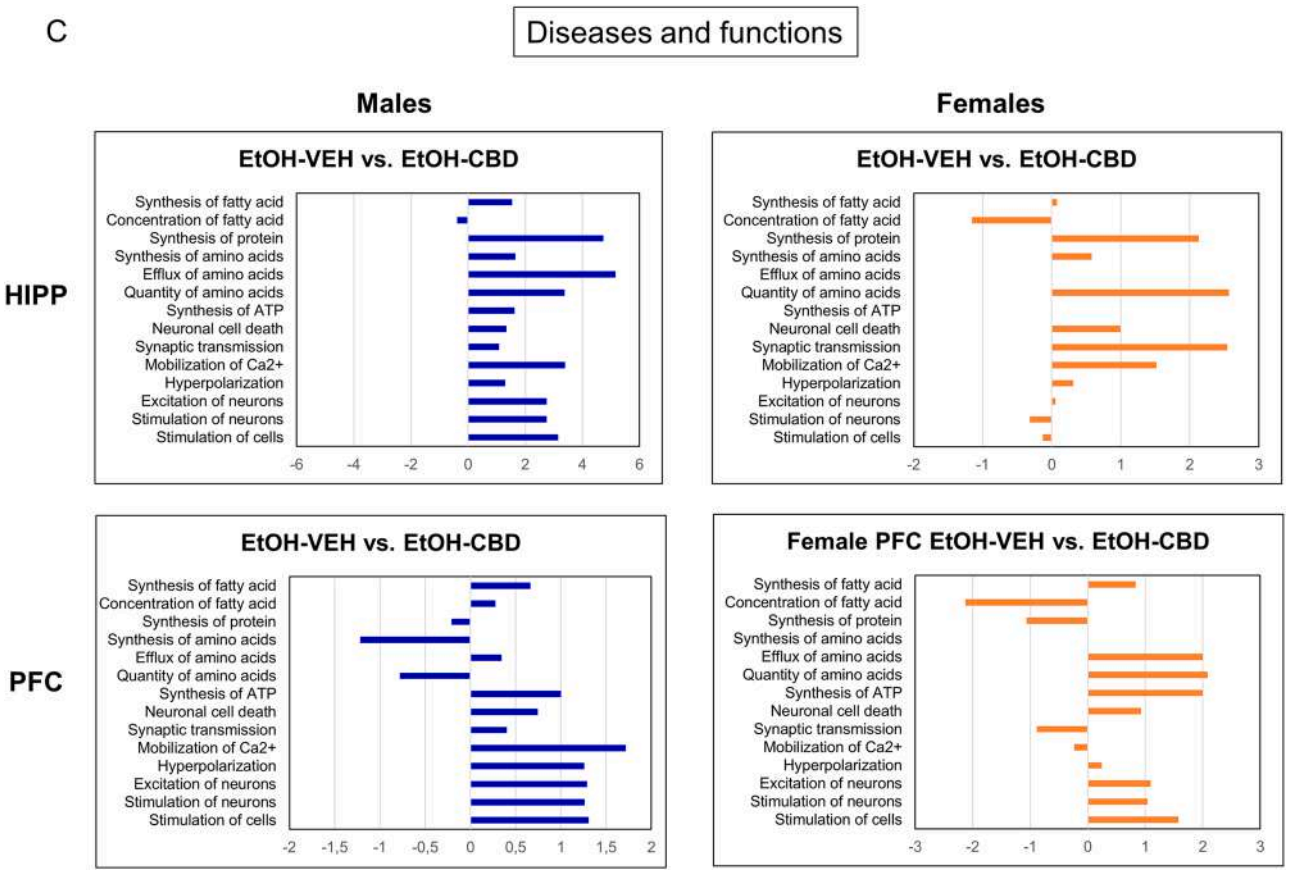

Fig. 14. (*continued*).

than 65 different targets, including the CB1 and CB2. Consequently, analyses of the gene expression of these targets were carried out in the HIPP, a brain region strongly involved in memory and emotions. Interestingly, female mice present lower *Cnr1* and *Cnr2* gene expressions under basal conditions, consistent with a previous report [60]. Sex-dependent differences were found in mice exposed to the FASD model. *Cnr1* gene expression increased in males and decreased in females. The higher emotional affectation of males in all the behavioral tests and the dysregulation of the HPA axis regular activity could be related to the increased gene expression of *Cnr1* in the HIPP. Chronic exposure to glucocorticoids, especially in the absence of the usual negative feedback of the HPA axis, has been associated with increased CB1 in the HIPP, which may explain the increase of the *Cnr1* gene expression in males exposed to the PAE protocol [61].

Moreover, several authors reported the sex-dependent actions of CB1 agonist or antagonist drugs in different experimental conditions that are consistent with the differential regulation of this brain target in males and females exposed to the FASD model [62–64]. In this study, CBD administration normalized the increase in *Cnr1* gene expression in males but not females. Nowadays, it is accepted that CBD act as an indirect agonist of CB1 by increasing anandamide levels through the blockade of its degradation and its reuptake [65]. In recent years, some authors also suggested that CBD could act as a negative allosteric modulator of CB1 [66]. Therefore, CBD could modulate *Cnr1* gene expression in males by normalizing endogenous cannabinoid signaling and regular HPA axis activity.

The cannabinoid receptor CB2 is another target of the endogenous cannabinoid system strongly involved in emotional regulation and alcohol intake [67,68]. In mice exposed to the FASD model, *Cnr2* gene expression was increased in both males and females, which could be related to the neuronal damage induced by alcohol and also to the emotional dysregulation, presenting more anxiogenic and depressive-like behaviors, emotional hyperreactivity, and cognitive impairment (Figs. 2 and 3). CBD's chronic and early administration modulates the increase of *Cnr2* gene expression in males but not females. Recent reports suggest that CBD acts as an inverse agonist or antagonist of CB2 and that these compounds show neuroprotective effects [69–72]. Therefore, it could be hypothesized that part of the positive effects observed in FASD model-exposed mice could be related to the neuroprotective effects of CBD through CB2 receptors. The ability of CBD to modulate sex-dependently endogenous cannabinoid signaling through its interaction with CB1 and CB2 receptors could be responsible, at least partially, for the positive behavioral effects observed after its administration. However, more studies are required to explore further the role of the endogenous cannabinoid system in the behavioral alterations associated with the FASD model and to identify the molecular mechanisms involved in the sex-dependent differences reported above.

The PPAR receptors are nuclear receptors activated by dietary lipids and endogenous ligands, such as long-chain saturated, polyunsaturated fatty acids, and lipid metabolic products [73]. The PPARβ/δ is the most abundant isotype of PPAR in the brain and presents an essential role in neuronal cell differentiation during development [74]. Indeed, the deletion of PPARβ/δ in mice induces neurodevelopmental and cognitive alterations [74–76]. In addition, recent studies reported the involvement of these receptors in animal models of neurological disorders [77], whereas agonist drugs of PPARβ/δ protect neurons and astrocytes and attenuate brain injury [78,79]. During the last few years, it has been an increased interest in evaluating the involvement of PPARβ/δ in different neuropsychiatric disorders. Some authors reported that PPARβ/δ agonism reduces the peripheral liver damage induced by chronic ethanol administration [80,81]. However, there is a lack of information about the potential changes of this target in the brain after alcohol exposure

and on the possible sex-dependent differences. Under basal conditions, males and females present similar *Pparβ/δ* gene expression in the HIPP. Hence, to explore the involvement of this target in the animal model of FASD, *Pparβ/δ* relative gene expression analyses were carried out in the HIPP. Interestingly, in both sexes, the PAE paradigm reduced the gene expression of this target, in agreement with a previous report on the involvement of this receptor in cognitive performance [76]. The treatment with CBD normalized this decrease in males but not in females. Fewer studies reported that the activation of PPARβ/δ receptors reduces the damage induced by chronic alcohol exposure and modulates the cognitive impairment in an animal model of Parkinson's disease [80, 82]. However, our study appears to be the first one demonstrating that CBD modulates the gene expression of *Pparβ/δ*. Considering the available literature, it is plausible to hypothesize that this action may be partially related to these mice's behavioral and cognitive improvement.

Memory impairment is one of the main symptoms described in human and animal models of FASD [83,84]. Our results revealed that male and female offspring exposed to alcohol during neurodevelopment present a significant deficit in learning and short and long-memory evaluated using the NOR and SDIA paradigms. Animal studies of hippocampal consequences of exposure to alcohol during pregnancy and lactation in the offspring are scarce. Abnormal morphophysiological traits established during gestation and early postnatal ages might be maintained throughout life and thereby be a risk factor for developing neuropsychiatric disorders later in life. Some studies reported that chronic alcohol exposure reduces hippocampal neurogenesis [85], and intermittent exposure to alcohol in adolescent rats produced a decrease in the neurogenesis in the DG of the hippocampus and an increase in cell death [86]. Immunohistochemical analyses were focused on studying cellular architecture, neuroplastic changes, and glutamatergic transmission. This study's results revealed a decrease in NeuN-ir cells in the CA_3 and the hilus of DG (Fig. 6A, B, C) in the mice exposed to the FASD model compared with controls.

Furthermore, the immunohistochemistry assays for BDNF showed a decrease in cell survival and plasticity in male and female mice exposed to the PAE protocol. BDNF-TrkB signaling pathway plays a critical role in activity-dependent synaptic plasticity related to memory and learning [87]. BDNF also regulates glutamate release. Impaired synaptic plasticity was found in glutamatergic synapses in diseases with compromised BDNF function [88]. Accordingly, the immunohistochemistry assay for NF200 (Figs. 9 and 10) revealed an alteration in the stabilization and maturation of neuronal connections in males and females ethanol-exposed groups, compared to controls. These synaptic alterations are glutamatergic. The immunohistochemistry assay for VGluT1 showed that the distribution of VGluT1-ir boutons in CA_3 and CA_1 of EtOH-VEH male and female mice was abnormal and revealed an alteration of the laminar distribution of excitatory input. In EtOH-VEH male and female mice, the VGluT1-ir bouton was decreased in strata oriens, lucidum and radiatum of CA_3 (double arrows in Fig. 12 B and Fig. 13 B) and stratum lacunosum-moleculare of CA_1 in comparison to W-VEH male mice (arrow in Fig. 12. A, B and Fig. 13A, B).

In the hippocampus, the DG receives its primary input from layer II of the entorhinal cortex via the perforant pathway. DG granule cells project mainly to the proximal apical dendrites (stratum lucidum) of CA_3 pyramidal cells, which in turn, project to ipsilateral apical dendrites (stratum radiatum) of CA_1 pyramidal cells through the Schaffer collaterals. Moreover, a dense associative excitatory network interconnects CA_3 to ipsilateral CA_3 and DG through recurrent connections [37,89] and to contralateral CA_3 and CA_1 through commissural connections [37]. Moreover, mossy cells, one of the primary cells of the hilus, are principal excitatory cells that provide long-range ipsilateral and commissural associational projections into the dentate gyrus [90,91]. The results showed that the excitatory synaptic loop is altered in EtOH-VEH male and female offspring exposed to alcohol during neurodevelopment. Decreased VGluT1-ir bouton density was found in (i) the stratum lucidum of CA_3 (receiving afferents from DG; Fig. 11A, B) and (ii) the strata lacunosum-moleculare (receiving afferents from layer III entorhinal cortex) and the proximal radiatum of CA_1 (receiving afferents from CA_3; Fig. 11A, B). In particular, the area occupied by VGluT1-ir boutons (mossy boutons) in strata oriens and lucidum of CA_3 was lower than in W-VEH female and male mice (double arrows Fig. 12A, B, D, E). Even though these alterations were more significant in males than females, both sexes showed cognitive impairment associated with a decrease in the number of neurons, impaired synaptic plasticity, and alterations in the excitatory synaptic loop in the HIPP.

CBD treatment during a peri-adolescence period can attenuate cognitive deficits induced by prenatal and lactation alcohol exposure in mice [21]. Immunohistochemistry for NeuN reveals that CBD administered from PND21 to PND56 enhanced hippocampal neurogenesis as there are similar NeuN-ir pyramidal neurons in the CA_3 and GD region in the EtOH-CBD group compared to W-VEH (arrow Fig. 6A, C, D, F) in both male and female mice (arrow in Fig. 6, A, C and Fig. 7A, C). Several dose-dependent studies showed that CBD enhanced neurogenesis in animal models [92–94]. CBD increased cell survival and plasticity since this compound was reported to increase BDNF expression [95]. In the model of FASD carried out in this study, CBD enhanced the labeling intensity of BDNF-ir in the EtOH-CBD group compared with EtOH-VEH male and female mice in the granular cells of the DG in the HIPP (double arrow in Fig. 9G, H, I, and Fig. 10G, H). Even the alteration of the stabilization and maturation of connections observed in the EtOH-VEH group compared to W-VEH normalized these effects with the treatment with CBD in male and female mice (Fig. 11A, B, C and Fig. 12A, B, C). Finally, CBD administration normalized the excitatory distribution in male and female perinatally ethanol-exposed mice (double arrow in Fig. 12 D, E, F and Fig. 13 D, E, F). It is important to note that the offspring receiving EtOH during gestation and lactation after CBD administration shows an increase in neurogenesis, cell survival, plasticity, and a reinstatement of the excitatory synaptic loop altered. In summary, CBD recovers the damage produced by the EtOH received during gestation and lactation.

As mentioned above, CBD has multiple targets in the mammalian cell, which probably contributes to explaining its plethora of effects. Some of the best-described targets of CBD are in mitochondrial metabolism (some examples are detailed in [96–99]). Targeted metabolomics studies were to elucidate the specific cellular target(s) underlying the observed effects of CBD in the FASD model. Specifically, 363 mitochondrial-related metabolites were targeted. The results showed significantly different metabolomic profiles between male and female mice in HIPP (Fig. 14). However, in the case of the PFC, these differences were only present in males (Fig. 14A). The different metabolomics profiles of the samples were confirmed in Fig. 14B, when we plotted the results using heat maps. Also, in this figure, the metabolic profile of the samples treated with EtOH-CBD was significantly different from those treated with EtOH-VEH, and it showed some similarities with the samples obtained from the EtOH-W group. All these data align with the previously discussed results, pointing towards a more potent effect of CBD in males than females under these experimental conditions.

Additionally, our heat maps (Fig. 14 B) showed that the primarily affected metabolites in the samples are not classically part of major mitochondrial processes, suggesting that mitochondria are not one of the main cellular targets for CBD in our models. This was confirmed by immunoblotting assays of some of the main proteins involved in regulating mammalian mitochondrial physiology and lipid peroxidation studies (Supplementary Figures). In the case of the immunoblots, proteins involved in mitochondrial dynamics, mitochondrial content, mitochondrial bioenergetics and the antioxidant system were assayed. Overall, no significant differences were found in the presence of these proteins in the samples, and when some differences were present, they were mainly in the PFC of females, which confirms the previous findings regarding the decreased effects of CBD in females. Lipid peroxidation, one of the main consequences of increased oxidative stress in the mammalian cell, was assayed by measuring the generation of MDA, a

classical subproduct of lipid peroxidation [100]. In this case, a significant increase of MDA was found in the HIPP of males treated with EtOH-CBD. The lack of other markers of mitochondrial increased oxidative stress or damage suggests that this increase might be compensated via antioxidant activation. However, the absence of the effect of this treatment on the main components of the electron transfer chain, as well as on some proteins with antioxidant properties in the mammalian cells (such as SOD2 and Sirt3), suggests that alternative pathways might underly this increase. This increase could be a direct consequence of changes in the lipidic metabolism (specifically of sphingolipids) induced by the treatment with CBD. Lipidic metabolism is also a cellular target of CBD [101].

Metabolomics data were analyzed using IPA (Fig. 15). The predictions obtained using this powerful software confirmed the findings from Fig. 14, suggesting that mitochondria are not the primary cellular target underlying the effects of CBD in the FASD model. Once again, these predictions showed more differences in the case of the males than in the females (Fig. 15A). Lastly, using IPA, the regulatory effects of CBD were analyzed in some of the main canonical pathways and diseases and functions related to the metabolism of CBD and/or with the observed effects of FASD in our samples (Fig. 15 B). The results showed that the treatment with CBD positively impacts some pathways involved in protein synthesis, lipid metabolism, and neuronal fitness. Interestingly, differences between male and female individuals were present, especially in the case of the PFC. For example, PFC from females is the only group of samples in which the treatment with CBD did not improve synaptic transmission. This figure also shows that the highest effects of CBD were found in males, which aligns with our previous results.

In summary, the metabolomics studies confirm the previous findings regarding the higher effect of CBD in the FASD model in male mice compared to females. Moreover, it suggests that mitochondria are not the primary cellular target for CBD in these studies. These results suggest that CBD acts through diverse targets, including some on lipidic and protein metabolism.

5. Conclusions

The results of the present study reveal that the early and chronic administration of CBD repairs the emotional and cognitive alterations observed in male and female mice exposed to the animal model of FASD. Likewise, CBD modulates sex-dependently the gene expression changes and metabolomic targets affected by the model exposure. Interestingly, the data suggest the absence of mitochondrial and oxidative targets in CBD-induced modulation, pointing out that lipid and protein metabolism could be another pathway involved in the cellular reparation observed after CBD chronic administration. The modulation of *Pparβ/δ* gene expression could be one of the multiple targets involved in CBD's induced cellular reparation and behavioral modulation. However, further studies are required to explore the real implication of this target in CBD's mechanism of action in this model of FASD. Taken together, these results strongly stimulate the possibility of performing clinical trials to evaluate the effects of CBD in children affected with FASD.

Funding

This work was supported by "Instituto de Salud Carlos III" PI21/00488 and RD21/0009/0008 to JM and Start-Up funds and a Global Grant from Rutgers University to MES.

CRediT authorship contribution statement

Ani Gasparyan: Formal analysis, Investigation, Methodology, Writing – original draft. **Daniela Navarro:** Methodology, Writing – original draft. **Daniela Navarroa:** Methodology, Writing – original draft. **Francisco Navarrete:** Methodology, Writing – original draft. **Amaya Austrich-Olivares:** Methodology. **Ernest R. Scoma:** Methodology, Writing – original draft. **Vedangi D. Hambardikar:** Methodology, Writing – original draft. **Gabriela B. Acosta:** Investigation, Methodology, Writing – original draft. María E. Solesio: Funding acquisition, Methodology, Supervision, Writing – original draft, Writing – review & editing. **Jorge Manzanares:** Conceptualization, Data curation, Formal analysis, Funding acquisition, Project administration, Supervision, Validation, Visualization, Writing – review & editing.

Data Availability

Data will be made available on request.

Acknowledgements

We kindly acknowledge Dr. Daniel Raftery and Dr. Fausto Carnevale-Neto (Northwest Metabolomics Research Center, University of Washington, Seattle, WA, USA) for their expert guidance in analyzing the metabolomics data.

Appendix A. Supporting information

Supplementary data associated with this article can be found in the online version at doi:10.1016/j.phrs.2023.106655.

References

[1] N. Dorrie, et al., Fetal alcohol spectrum disorders, Eur. Child Adolesc. Psychiatry 23 (10) (2014) 863–875.
[2] F. Ehrhart, et al., Review and gap analysis: molecular pathways leading to fetal alcohol spectrum disorders, Mol. Psychiatry 24 (1) (2019) 10–17.
[3] J.J. Joseph, M. Mela, J. Pei, Aggressive behaviour and violence in children and adolescents with FASD: a synthesizing review, Clin. Psychol. Rev. 94 (2022), 102155.
[4] K.E. Boschen, A.Y. Klintsova, Neurotrophins in the brain: interaction with alcohol exposure during development, Vitam. Horm. 104 (2017) 197–242.
[5] C.D. Coles, Discriminating the effects of prenatal alcohol exposure from other behavioral and learning disorders, Alcohol Res Health 34 (1) (2011) 42–50.
[6] S. Lange, et al., Global prevalence of fetal alcohol spectrum disorder among children and youth: a systematic review and meta-analysis, JAMA Pedia 171 (10) (2017) 948–956.
[7] P.A. May, et al., Prevalence and characteristics of fetal alcohol spectrum disorders, Pediatrics 134 (5) (2014) 855–866.
[8] P.A. May, et al., Prevalence of fetal alcohol spectrum disorders in 4 US communities, JAMA 319 (5) (2018) 474–482.
[9] S.N. Mattson, G.A. Bernes, L.R. Doyle, Fetal alcohol spectrum disorders: a review of the neurobehavioral deficits associated with prenatal alcohol exposure, Alcohol Clin. Exp. Res 43 (6) (2019) 1046–1062.
[10] J.H. Hannigan, R.F. Berman, Amelioration of fetal alcohol-related neurodevelopmental disorders in rats: exploring pharmacological and environmental treatments, Neurotoxicol. Teratol. 22 (1) (2000) 103–111.
[11] J.E. Khoury, B. Jamieson, K. Milligan, Risk for childhood internalizing and externalizing behavior problems in the context of prenatal alcohol exposure: a meta-analysis and comprehensive examination of moderators, Alcohol Clin. Exp. Res (2018).
[12] M. Simakova, et al., Gestational age-dependent interplay between endocannabinoid receptors and alcohol in fetal cerebral arteries, J. Drug Alcohol Res (2019) **8**.
[13] S. Subbanna, et al., Anandamide-CB1 receptor signaling contributes to postnatal ethanol-induced neonatal neurodegeneration, adult synaptic, and memory deficits, J. Neurosci. 33 (15) (2013) 6350–6366.
[14] S. Subbanna, et al., Ethanol exposure induces neonatal neurodegeneration by enhancing CB1R Exon1 histone H4K8 acetylation and up-regulating CB1R function causing neurobehavioral abnormalities in adult mice, Int J. Neuropsychopharmacol. 18 (2014) 5.
[15] S. Subbanna, et al., Postnatal ethanol exposure alters levels of 2-arachidonylglycerol-metabolizing enzymes and pharmacological inhibition of monoacylglycerol lipase does not cause neurodegeneration in neonatal mice, J. Neurochem 134 (2) (2015) 276–287.
[16] O. Seleverstov, et al., Maternal alcohol exposure during mid-pregnancy dilates fetal cerebral arteries via endocannabinoid receptors, Alcohol 61 (2017) 51–61.
[17] A. Viudez-Martinez, et al., Cannabidiol does not display drug abuse potential in mice behavior, Acta Pharm. Sin. 40 (3) (2019) 358–364.
[18] A.A. Izzo, et al., Non-psychotropic plant cannabinoids: new therapeutic opportunities from an ancient herb, Trends Pharm. Sci. 30 (10) (2009) 515–527.
[19] S. Elsaid, S. Kloiber, B. Le Foll, Effects of cannabidiol (CBD) in neuropsychiatric disorders: a review of pre-clinical and clinical findings, Prog. Mol. Biol. Transl. Sci. 167 (2019) 25–75.

[20] G. Koren, R. Cohen, O. Sachs, Use of cannabis in fetal alcohol spectrum disorder, Cannabis Cannabinoid Res. 6 (1) (2021) 74–76.
[21] A. Garcia-Baos, et al., Cannabidiol attenuates cognitive deficits and neuroinflammation induced by early alcohol exposure in a mice model, Biomed. Pharm. 141 (2021), 111813.
[22] C. Kilkenny, et al., Improving bioscience research reporting: the ARRIVE guidelines for reporting animal research, J. Pharm. Pharm. 1 (2) (2010) 94–99.
[23] N. Percie du Sert, et al., The ARRIVE guidelines 2.0: updated guidelines for reporting animal research, PLoS Biol. 18 (7) (2020), e3000410.
[24] A. Viudez-Martinez, et al., Cannabidiol reduces ethanol consumption, motivation and relapse in mice, Addict. Biol. 23 (1) (2018) 154–164.
[25] J. Crawley, F.K. Goodwin, Preliminary report of a simple animal behavior model for the anxiolytic effects of benzodiazepines, Pharm. Biochem. Behav. 13 (2) (1980) 167–170.
[26] A. Gasparyan, F. Navarrete, J. Manzanares, Cannabidiol and sertraline regulate behavioral and brain gene expression alterations in an animal model of PTSD, Front Pharm. 12 (2021), 694510.
[27] A. Austrich-Olivares, et al., Cannabinoid CB1 receptor involvement in the actions of CBD on anxiety and coping behaviors in mice, Pharmaceuticals 15 (4) (2022).
[28] S.R. Bodnoff, et al., The effects of chronic antidepressant treatment in an animal model of anxiety, Psychopharmacol. (Berl.) 95 (3) (1988) 298–302.
[29] J.M. Vaugeois, et al., Individual differences in response to imipramine in the mouse tail suspension test, Psychopharmacol. (Berl.) 134 (4) (1997) 387–391.
[30] A. Ortega-Alvaro, et al., Deletion of CB2 cannabinoid receptor induces schizophrenia-related behaviors in mice, Neuropsychopharmacology 36 (7) (2011) 1489–1504.
[31] A. Ennaceur, N. Neave, J.P. Aggleton, Spontaneous object recognition and object location memory in rats: the effects of lesions in the cingulate cortices, the medial prefrontal cortex, the cingulum bundle and the fornix, Exp. Brain Res. 113 (3) (1997) 509–519.
[32] I. Izquierdo, et al., Differential involvement of cortical receptor mechanisms in working, short-term and long-term memory, Behav. Pharm. 9 (5–6) (1998) 421–427.
[33] G. Paxinos, K.B.J. Franklin, The mouse brain in stereotaxic coordinates. Compact, second ed., Boston: Elsevier Academic Press, Amsterdam, 2004.
[34] M. Palkovits, Punch sampling biopsy technique, Methods Enzym. 103 (1983) 368–376.
[35] F. Navarrete, J.M. Perez-Ortiz, J. Manzanares, Pregabalin- and topiramate-mediated regulation of cognitive and motor impulsivity in DBA/2 mice, Br. J. Pharm. 167 (1) (2012) 183–195.
[36] K.J. Livak, T.D. Schmittgen, Analysis of relative gene expression data using real-time quantitative PCR and the 2(-Delta Delta C(T)) Method, Methods 25 (4) (2001) 402–408.
[37] D.G. Amaral, M.P. Witter, Hippocampal formation. The Rat Nervous System, second ed., Academic Press, San Diego, CA, 1995.
[38] A. Baltanas, et al., The senescence-accelerated mouse prone-8 (SAM-P8) oxidative stress is associated with upregulation of renal NADPH oxidase system, J. Physiol. Biochem 69 (4) (2013) 927–935.
[39] M.E. Solesio, et al., Depletion of mitochondrial inorganic polyphosphate (polyP) in mammalian cells causes metabolic shift from oxidative phosphorylation to glycolysis, Biochem J. 478 (8) (2021) 1631–1646.
[40] A. Ternianov, et al., Overexpression of CB2 cannabinoid receptors results in neuroprotection against behavioral and neurochemical alterations induced by intracaudate administration of 6-hydroxydopamine, Neurobiol. Aging 33 (2) (2012) 421, e1-16.
[41] V. Hambardikar, et al., Enzymatic depletion of mitochondrial inorganic polyphosphate (polyP) increases the generation of reactive oxygen species (ROS) and the activity of the pentose phosphate pathway (PPP) in mammalian cells, Antioxidants 11 (4) (2022).
[42] M. Guitart-Mampel, et al., Mitochondrial Inorganic Polyphosphate (polyP) Is a Potent Regulator of Mammalian Bioenergetics in SH-SY5Y Cells: A Proteomics and Metabolomics Study, Front Cell Dev. Biol. 10 (2022), 833127.
[43] C. Mathon, et al., Impact of sample preparation upon intracellular metabolite measurements in 3D cell culture systems, Metabolomics 15 (6) (2019) 92.
[44] J.P. Meador, et al., Metabolomic profiling for juvenile Chinook salmon exposed to contaminants of emerging concern, Sci. Total Environ. 747 (2020), 141097.
[45] S. Atalay, I. Jarocka-Karpowicz, E. Skrzydlewska, Antioxidative and anti-inflammatory properties of cannabidiol, Antioxid. (Basel) 9 (1) (2019).
[46] J.Z. Chan, R.E. Duncan, Regulatory effects of cannabidiol on mitochondrial functions: a review, Cells 10 (5) (2021).
[47] P.S. Brocardo, et al., Anxiety- and depression-like behaviors are accompanied by an increase in oxidative stress in a rat model of fetal alcohol spectrum disorders: Protective effects of voluntary physical exercise, Neuropharmacology 62 (4) (2012) 1607–1618.
[48] C. Banuelos, et al., Altered spatial learning and delay discounting in a rat model of human third trimester binge ethanol exposure, Behav. Pharm. 23 (1) (2012) 54–65.
[49] P.S. Hunt, R.C. Barnet, An animal model of fetal alcohol spectrum disorder: trace conditioning as a window to inform memory deficits and intervention tactics, Physiol. Behav. 148 (2015) 36–44.
[50] S.M. Huebner, et al., Maternal iron deficiency worsens the associative learning deficits and hippocampal and cerebellar losses in a rat model of fetal alcohol spectrum disorders, Alcohol Clin. Exp. Res 39 (11) (2015) 2097–2107.
[51] P.J. Holman, et al., Altered social recognition memory and hypothalamic neuropeptide expression in adolescent male and female rats following prenatal alcohol exposure and/or early-life adversity, Psychoneuroendocrinology 126 (2021), 105146.
[52] M. Endres, et al., Prevention of alcohol-induced developmental delays and learning abnormalities in a model of fetal alcohol syndrome, Am. J. Obstet. Gynecol. 193 (3 Pt 2) (2005) 1028–1034.
[53] L. Cantacorps, et al., Altered brain functional connectivity and behaviour in a mouse model of maternal alcohol binge-drinking, Prog. Neuropsychopharmacol. Biol. Psychiatry 84 (Pt A) (2018) 237–249.
[54] A. Ieraci, D.G. Herrera, Early postnatal ethanol exposure in mice induces sex-dependent memory impairment and reduction of hippocampal NMDA-R2B expression in adulthood, Neuroscience 427 (2020) 105–115.
[55] R.C. Lawrence, N.K. Otero, S.J. Kelly, Selective effects of perinatal ethanol exposure in medial prefrontal cortex and nucleus accumbens, Neurotoxicol Teratol. 34 (1) (2012) 128–135.
[56] M. Lopatynska-Mazurek, et al., Rapamycin improves recognition memory and normalizes amino-acids and amines levels in the hippocampal dentate gyrus in adult rats exposed to ethanol during the neonatal period, Biomolecules 11 (3) (2021).
[57] C.R. Goodlett, S.D. Peterson, Sex differences in vulnerability to developmental spatial learning deficits induced by limited binge alcohol exposure in neonatal rats, Neurobiol. Learn Mem. 64 (3) (1995) 265–275.
[58] A. Locci, et al., Sex differences in CRF1, CRF, and CRFBP expression in C57BL/6J mouse brain across the lifespan and in response to acute stress, J. Neurochem 158 (4) (2021) 943–959.
[59] A. Viudez-Martinez, M.S. Garcia-Gutierrez, J. Manzanares, Gender differences in the effects of cannabidiol on ethanol binge drinking in mice, Addict. Biol. 25 (3) (2020), e12765.
[60] X. Liu, et al., Sexual dimorphic distribution of cannabinoid 1 receptor mRNA in adult C57BL/6J mice, J. Comp. Neurol. 528 (12) (2020) 1986–1999.
[61] M.N. Hill, et al., Prolonged glucocorticoid treatment decreases cannabinoid CB1 receptor density in the hippocampus, Hippocampus 18 (2) (2008) 221–226.
[62] H.A. Chang, W. Dai, S.S. Hu, Sex differences in cocaine-associated memory: the interplay between CB(1), mGluR5, and estradiol, Psychoneuroendocrinology 133 (2021), 105366.
[63] B.K. Keeney, et al., Sex differences in cannabinoid receptor-1 (CB1) pharmacology in mice selectively bred for high voluntary wheel-running behavior, Pharm. Biochem Behav. 101 (4) (2012) 528–537.
[64] R.M. Craft, et al., Sex differences in cannabinoid 1 vs. cannabinoid 2 receptor-selective antagonism of antinociception produced by delta9-tetrahydrocannabinol and CP55,940 in the rat, J. Pharm. Exp. Ther. 340 (3) (2012) 787–800.
[65] T. Bisogno, et al., Molecular targets for cannabidiol and its synthetic analogues: effect on vanilloid VR1 receptors and on the cellular uptake and enzymatic hydrolysis of anandamide, Br. J. Pharm. 134 (4) (2001) 845–852.
[66] M. Tham, et al., Allosteric and orthosteric pharmacology of cannabidiol and cannabidiol-dimethylheptyl at the type 1 and type 2 cannabinoid receptors, Br. J. Pharm. 176 (10) (2019) 1455–1469.
[67] M.S. Garcia-Gutierrez, et al., Depression-resistant endophenotype in mice overexpressing cannabinoid CB(2) receptors, Br. J. Pharm. 160 (7) (2010) 1773–1784.
[68] F. Navarrete, M.S. Garcia-Gutierrez, J. Manzanares, Pharmacological regulation of cannabinoid CB2 receptor modulates the reinforcing and motivational actions of ethanol, Biochem Pharm. 157 (2018) 227–234.
[69] A. Thomas, et al., Cannabidiol displays unexpectedly high potency as an antagonist of CB1 and CB2 receptor agonists in vitro, Br. J. Pharm. 150 (5) (2007) 613–623.
[70] Y. Yu, et al., Inverse agonism of cannabinoid receptor type 2 confers anti-inflammatory and neuroprotective effects following status epileptics, Mol. Neurobiol. 57 (6) (2020) 2830–2845.
[71] J. Zhao, et al., Activation of cannabinoid receptor 2 protects rat hippocampal neurons against Abeta-induced neuronal toxicity, Neurosci. Lett. 735 (2020), 135207.
[72] M. Scheiner, et al., Dual-acting cholinesterase-human cannabinoid receptor 2 ligands show pronounced neuroprotection in vitro and overadditive and disease-modifying neuroprotective effects in vivo, J. Med Chem. 62 (20) (2019) 9078–9102.
[73] A.K. Strosznajder, et al., Recent insights on the role of PPAR-beta/delta in neuroinflammation and neurodegeneration, and its potential target for therapy, Neuromolecular Med 23 (1) (2021) 86–98.
[74] M.G. Hall, L. Quignodon, B. Desvergne, Peroxisome proliferator-activated receptor beta/delta in the brain: facts and hypothesis, PPAR Res 2008 (2008), 780452.
[75] A. Sanjay, Sharma, H.J. Lee, Role of phytoconstituents as PPAR agonists: implications for neurodegenerative disorders, Biomedicines 9 (12) (2021).
[76] T. Espinosa-Jimenez, et al., Peroxisomal proliferator-activated receptor beta/delta deficiency induces cognitive alterations, Front Pharm. 13 (2022), 902047.
[77] A.S. Dickey, et al., PPAR-delta is repressed in Huntington's disease, is required for normal neuronal function and can be targeted therapeutically, Nat. Med 22 (1) (2016) 37–45.
[78] S. Aleshin, G. Reiser, Peroxisome proliferator-activated receptor beta/delta (PPARbeta/delta) protects against ceramide-induced cellular toxicity in rat brain astrocytes and neurons by activation of ceramide kinase, Mol. Cell Neurosci. 59 (2014) 127–134.
[79] X. Tang, et al., Activation of PPAR-beta/delta attenuates brain injury by suppressing inflammation and apoptosis in a collagenase-induced intracerebral hemorrhage mouse model, Neurochem Res 45 (4) (2020) 837–850.

[80] C.Q. Xu, et al., Chronic ethanol-induced impairment of wnt/beta-catenin signaling is attenuated by PPAR-delta agonist, Alcohol Clin. Exp. Res 39 (6) (2015) 969–979.
[81] M. Goudarzi, et al., PPARbeta/delta modulates ethanol-induced hepatic effects by decreasing pyridoxal kinase activity, Toxicology 311 (3) (2013) 87–98.
[82] N.R. Das, et al., A PPAR-beta/delta agonist is neuroprotective and decreases cognitive impairment in a rodent model of Parkinson's disease, Curr. Neurovasc Res. 11 (2) (2014) 114–124.
[83] M.L. Brady, A.M. Allan, K.K. Caldwell, A limited access mouse model of prenatal alcohol exposure that produces long-lasting deficits in hippocampal-dependent learning and memory, Alcohol Clin. Exp. Res 36 (3) (2012) 457–466.
[84] J.A. Kable, et al., Neurobehavioral disorder associated with prenatal alcohol exposure (ND-PAE): proposed DSM-5 diagnosis, Child Psychiatry Hum. Dev. 47 (2) (2016) 335–346.
[85] J. He, et al., Chronic alcohol exposure reduces hippocampal neurogenesis and dendritic growth of newborn neurons, Eur. J. Neurosci. 21 (10) (2005) 2711–2720.
[86] R.P. Vetreno, F.T. Crews, Binge ethanol exposure during adolescence leads to a persistent loss of neurogenesis in the dorsal and ventral hippocampus that is associated with impaired adult cognitive functioning, Front Neurosci. 9 (2015) 35.
[87] J.B. Yin, et al., Neurochemical properties of BDNF-containing neurons projecting to rostral ventromedial medulla in the ventrolateral periaqueductal gray, Front Neural Circuits 8 (2014) 137.
[88] A.L. Carvalho, et al., Role of the brain-derived neurotrophic factor at glutamatergic synapses, Br. J. Pharm. 153 (Suppl 1) (2008) S310–S324.
[89] J.E. Lisman, L.M. Talamini, A. Raffone, Recall of memory sequences by interaction of the dentate and CA3: a revised model of the phase precession, Neural Netw. 18 (9) (2005) 1191–1201.
[90] D.G. Amaral, A Golgi study of cell types in the hilar region of the hippocampus in the rat, J. Comp. Neurol. 182 (4 Pt 2) (1978) 851–914.
[91] T.F. Freund, G. Buzsaki, Interneurons of the hippocampus, Hippocampus 6 (4) (1996) 347–470.
[92] A.P. Schiavon, et al., Influence of single and repeated cannabidiol administration on emotional behavior and markers of cell proliferation and neurogenesis in non-stressed mice, Prog. Neuropsychopharmacol. Biol. Psychiatry 64 (2016) 27–34.
[93] M.V. Fogaca, et al., The anxiolytic effects of cannabidiol in chronically stressed mice are mediated by the endocannabinoid system: Role of neurogenesis and dendritic remodeling, Neuropharmacology 135 (2018) 22–33.
[94] M.A. Lujan, O. Valverde, The pro-neurogenic effects of cannabidiol and its potential therapeutic implications in psychiatric disorders, Front Behav. Neurosci. 14 (2020) 109.
[95] A.J. Sales, et al., Cannabidiol induces rapid and sustained antidepressant-like effects through increased BDNF signaling and synaptogenesis in the prefrontal cortex, Mol. Neurobiol. 56 (2) (2019) 1070–1081.
[96] D. Ryan, et al., Cannabidiol targets mitochondria to regulate intracellular Ca2+ levels, J. Neurosci. 29 (7) (2009) 2053–2063.
[97] C. Gross, et al., Cannabidiol induces apoptosis and perturbs mitochondrial function in human and canine glioma cells, Front Pharm. 12 (2021), 725136.
[98] S.S. Valvassori, et al., Acute and chronic administration of cannabidiol increases mitochondrial complex and creatine kinase activity in the rat brain, Braz. J. Psychiatry 35 (4) (2013) 380–386.
[99] Z. Fisar, N. Singh, J. Hroudova, Cannabinoid-induced changes in respiration of brain mitochondria, Toxicol. Lett. 231 (1) (2014) 62–71.
[100] S. Gawel, et al., [Malondialdehyde (MDA) as a lipid peroxidation marker], Wiad. Lek. 57 (9–10) (2004) 453–455.
[101] T. Charytoniuk, et al., Cannabidiol - a phytocannabinoid that widely affects sphingolipid metabolism under conditions of brain insulin resistance, Biomed. Pharm. 142 (2021), 112057.